August, 1997

The Lagrangian spectral relaxation model of the scalar dissipation in homogeneous turbulence

Rodney O. Fox, *Kansas State University*

The Lagrangian spectral relaxation model of the scalar dissipation in homogeneous turbulence

R. O. Fox

Citation: Physics of Fluids (1994-present) **9**, 2364 (1997); doi: 10.1063/1.869357
View online: http://dx.doi.org/10.1063/1.869357
View Table of Contents: http://scitation.aip.org/content/aip/journal/pof2/9/8?ver=pdfcov
Published by the AIP Publishing

The Lagrangian spectral relaxation model of the scalar dissipation in homogeneous turbulence

R. O. Fox[a)]
Department of Chemical Engineering, Kansas State University, Manhattan, Kansas 66506

(Received 24 January 1997; accepted 7 April 1997)

Lagrangian pdf methods are employed to extend the spectral relaxation (SR) model of the scalar dissipation of an inert, passive scalar ($1 \leqslant Sc$) in homogeneous turbulence. The Lagrangian spectral relaxation (LSR) model divides wavenumber space into a finite number (the total number depending on the Taylor-scale Reynolds number R_λ and the Schmidt number Sc) of wavenumber bands whose time constants are determined from the mean turbulent kinetic energy and instantaneous turbulent energy dissipation rate. The LSR model accounts for the evolution of the scalar spectrum (viz., pdf) from an arbitrary initial shape to its fully developed form. The effect of turbulent-frequency fluctuations on the instantaneous scalar dissipation rate following a Kolmogorov-scale fluid particle is incorporated into the LSR model through a Lagrangian pdf model for the turbulent frequency. Model results are compared with DNS data for passive scalar mixing in stationary, isotropic turbulence. Two distinct causes of non-Gaussian scalar statistics are investigated: small-scale intermittency due to scalar-dissipation fluctuations at scales near the Kolmogorov scale, and transient large-scale inhomogeneities due to the form of the initial scalar spectrum at scales near the integral scale. Despite the absence of fitting parameters, the LSR model shows satisfactory agreement with available DNS data for both types of flows. © *1997 American Institute of Physics.* [S1070-6631(97)01108-2]

I. INTRODUCTION

Like the turbulent dissipation rate, the scalar dissipation rate provides information about scalar time and length scales needed to close the scalar variance equation, and is a key quantity in the modeling of both inert and reacting turbulent scalar fields.[1–6] Nearly all currently employed models for scalar mixing ranging from simple moment closures to full probability density function (pdf) simulations require information concerning the coupling between the turbulence time scales and the scalar time scales for closure. Ample experimental and direct numerical simulation (DNS) data exist to show that the usual assumption of a direct proportionality between these time scales is often unjustified and that, in reality, the velocity-to-scalar time-scale ratio varies widely according to the flow under consideration and with time, depending in particular on the initial scalar-to-mechanical integral-scale ratio.[7–10]

In an earlier work[4] the spectral relaxation (SR) model of the *mean* scalar dissipation rate was introduced and shown to successfully account for the effect of the velocity spectrum on the relaxation of the scalar spectrum from an arbitrary initial form in both stationary and decaying turbulence. The SR model contains a range of turbulent time (length) scales and thus accounts for the cascade of scalar energy from large to small scales. This division of physical mixing processes according to their characteristic length scales removes all fitting parameters, replacing them with physical constants that characterize the fundamental processes of turbulent vortex stretching and molecular dissipation. The objective of the present work is to extend the SR model using Lagrangian pdf methods to account for Kolmogorov-scale fluctuations in the vortex-stretching rate, and their effect on the one-point scalar and scalar dissipation statistics in homogeneous turbulence.

Lagrangian pdf methods combine pdf methods with stochastic Lagrangian models to provide a computationally tractable method for calculating the statistics of inhomogeneous turbulent flows of practical importance.[11] Models at the level of the velocity, turbulent frequency, composition Lagrangian pdf represent the current state of the art[12] and provide a description of scalar transport in high Reynolds-number turbulent flows. The lack of a dynamic model for the scalar dissipation rate, however, limits their application to fully developed (equilibrium) scalar field decay in stationary turbulence and to flows for which knowledge of the mean (as opposed to *instantaneous*) scalar dissipation rate suffices. (Reactive flows dominated by ignition and extinction events[13–18] are an example of a class of flows requiring a dynamic model like the one developed in this work.) With the addition of the Lagrangian spectral relaxation (LSR) model, this limitation will be lifted and the resulting *velocity, turbulent frequency, composition, scalar dissipation* Lagrangian pdf description will be applicable to cases with arbitrary initial scalar length-scale distributions, and provide one-point statistics and a *time history* for the scalar dissipation in each fluid particle.

The remainder of this work is arranged as follows. In Sec. II the SR model is reviewed and minor modifications of the original model are introduced. The LSR model is presented in Sec. III in the form of a set of stochastic differential equations for the mean scalar dissipation *conditioned on* a given turbulent-frequency time history: $\mathscr{W}(t)=\{\omega^*(s)\,|\,s \in (-\infty,t]\}$, where $\omega^*(t)$ is the turbulent dissipation in a Lagrangian fluid particle divided by the mean turbulent ki-

[a)]On sabbatical leave at the Laboratoire de Mécanique des Fluides Numérique, CORIA UMR 6614 CNRS—Université & INSA de Rouen, 76801 Saint Etienne du Rouvray, France.

 1070-6631/97/9(8)/2364/23/$10.00

netic energy at the particle location. The LSR model, combined with the Fokker–Planck model,[19,20] is applied to study passive scalar mixing in stationary, isotropic turbulence in Sec. IV, and the results are compared to DNS data[21,22] for joint one-point statistics of the scalar, scalar dissipation, and turbulent frequency. Conclusions are drawn in Sec. V.

II. SPECTRAL RELAXATION MODEL

The SR model was introduced to improve the description of the influence of the velocity field on the scalar dissipation rate in turbulent flows. The model explicitly accounts for the relaxation of a non-equilibrium scalar spectrum to its final self-similar form through the actions of turbulent mixing. Since many fast reactions take place in the non-equilibrium regime,[23,24] the relaxation period is particularly important for reacting flows where neglect of the transient behavior can lead to serious prediction errors.[25]

Turbulent mixing of a passive scalar can be described by the Reynolds-averaged moment equations for the scalar mean and variance. For a homogeneous scalar field with a uniform mean scalar gradient and molecular diffusivity Γ, the governing equations become, respectively,

$$\frac{D\langle\phi\rangle}{Dt}=0 \tag{1}$$

and

$$\frac{D\langle\phi'^2\rangle}{Dt}=2S_{\phi^2}-2\langle\epsilon_\phi\rangle, \tag{2}$$

where the mean convected derivative is defined by (repeated indices imply summation)

$$\frac{D}{Dt}=\frac{\partial}{\partial t}+\langle U_i\rangle\frac{\partial}{\partial x_i}, \tag{3}$$

the mean scalar dissipation by

$$\langle\epsilon_\phi\rangle=\left\langle\Gamma\frac{\partial\phi'}{\partial x_i}\frac{\partial\phi'}{\partial x_i}\right\rangle, \tag{4}$$

the scalar variance source by

$$S_{\phi^2}=-\langle u_i\phi'\rangle\frac{\partial\langle\phi\rangle}{\partial x_i}, \tag{5}$$

and $u_i=U_i-\langle U_i\rangle$, $\phi'=\phi-\langle\phi\rangle$ are the fluctuation fields. Note that both the scalar dissipation and the scalar variance source terms are unclosed.

The mean scalar dissipation rate is defined in terms of the mean scalar dissipation by

$$\langle r_\phi\rangle=\frac{\langle\epsilon_\phi\rangle}{\langle\phi'^2\rangle}. \tag{6}$$

The governing equation for the scalar gradient can be used to find an expression for the mean scalar dissipation.[4] The resulting expression contains terms corresponding to production by the mean scalar gradient, turbulent vortex stretching of the fluctuating scalar gradient, and to molecular dissipation, all of which must be modeled. The SR model closes the mean scalar dissipation rate equation by

$$\frac{D\langle r_\phi\rangle}{Dt}=2C_DRe_1\langle\omega\rangle\frac{T_D}{\langle\phi'^2\rangle}+2C_sRe_1\langle\omega\rangle\langle r_\phi\rangle-2C_d\langle r_\phi\rangle_o\langle r_\phi\rangle+2D_\phi\langle r_\phi\rangle, \tag{7}$$

where the mean turbulent frequency is defined by

$$\langle\omega\rangle=\frac{\langle\epsilon\rangle}{\langle k\rangle}, \tag{8}$$

the turbulent Reynolds number by

$$Re_1=\frac{\langle k\rangle}{\sqrt{\nu\langle\epsilon\rangle}}=0.3873R_\lambda \tag{9}$$

(R_λ is the Taylor-scale Reynolds number), $C_D=C_s/(C_d-1)=0.25$, $C_s=0.5/N_z$, and $C_d=1+2/N_z$, where $1\leqslant N_z\leqslant 3$ is the effective dimension of the scalar field [see the discussion after Eq. (90)].

In the SR model, C_s is Batchelor's constant,[26,27] and has been verified using DNS.[28] The molecular-diffusion constant C_d has been determined by forcing the model to agree with the pure diffusion case[20] where $\langle\phi'^2\rangle\sim t^{-N_z/2}$ for large t. The symbol T_D denotes the flux of scalar energy from wavenumbers below the scalar-dissipation wavenumber, $\kappa_D=C_D^{3/2}\kappa_B=\kappa_B/8$ where $\kappa_B=Sc^{1/2}\kappa_K$ is the Batchelor-scale wavenumber[27] and $\kappa_K=2\pi(\langle\epsilon\rangle/\nu^3)^{1/4}$ is the Kolmogorov-scale wavenumber.[31] The symbol D_ϕ is defined by

$$D_\phi=-\frac{1}{2\langle\phi'^2\rangle}\frac{d\langle\phi'^2\rangle}{dt}=\langle r_\phi\rangle-\frac{S_{\phi^2}}{\langle\phi'^2\rangle}, \tag{10}$$

and the characteristic molecular dissipation rate, $\langle r_\phi\rangle_o$ is given by Eq. (24) below. $\langle k\rangle$ and $\langle\epsilon\rangle$ are the *mean* turbulent kinetic energy and dissipation rate, respectively, and ν is the kinematic viscosity.

Physically, the first two terms of the right-hand side of Eq. (7) represent a closure for the effect of the turbulent velocity field on the scalar gradient. Turbulent advection works to decrease the scalar length scale by pushing more scalar energy to larger wavenumbers. The first term thus results from scalar energy transported from large to small scales, and the second term models small-scale straining of the scalar field by the vorticity field. The third term on the right-hand side is a closure for the effect of molecular dissipation on the scalar gradient. At spectral equilibrium, $T_D/\langle\phi'^2\rangle$ is constant and the right-hand side of Eq. (7) is null as transport of scalar energy from large to small scales is exactly balanced by molecular dissipation.

The SR model describes the non-equilibrium transport of scalar energy as a cascade process from large to small scales. In order to provide a computationally tractable model, spectral transport is assumed to be local in scalar wavenumber space,[29,30] and the turbulent velocity spectrum is assumed to be fully developed (i.e., equilibrium turbulence).[31–33] In the original formulation of the model, additional dynamical variables were then introduced that correspond to ''potential'' scalar dissipations.[4] These variables were referred to as potential scalar dissipations because they are formed by multi-

plying the fraction of the scalar spectrum, $E_\phi(\kappa,t)$, in a finite band of wavenumbers $[\kappa_{i,j-1},\kappa_{i,j})$ by a factor proportional to $\Gamma\kappa_D^2$:

$$\langle \epsilon_{i,j}\rangle = C_D Re_1 \langle\omega\rangle \langle \phi_{i,j}'^2\rangle, \tag{11}$$

where

$$\langle \phi_{i,j}'^2\rangle = \int_{\kappa_{i,j-1}}^{\kappa_{i,j}} E_\phi(\kappa,t)\,d\kappa, \tag{12}$$

and $\kappa_{i,j}$ is the upper-cutoff wavenumber of the jth substage of the ith spectral subrange defined below. Here, in order to make the relationship between the SR model variables and the scalar spectrum more transparent, we shall work with the model in terms of $\langle \phi_{i,j}'^2\rangle$ or, equivalently, in terms of the fraction of the scalar energy in a wavenumber band:

$$\langle \varsigma_{i,j}\rangle = \frac{\langle \phi_{i,j}'^2\rangle}{\langle \phi'^2\rangle}. \tag{13}$$

Note that by definition $0\leqslant\langle\varsigma_{i,j}\rangle\leqslant 1$ and the sum of all fractions is unity.

In the SR model, the scalar energy in the ith stage of the cascade is denoted by $\langle \phi_i'^2\rangle$ and in the (i,j)th substage, by $\langle \phi_{i,j}'^2\rangle$. The cascade is composed of three principal stages representing the following.

(1) Transport from wavenumbers below the integral-scale wavenumber of the turbulent velocity field to $\kappa_0 = Re_1^{-3/2}\kappa_K$, i.e., wavenumber band $[0,\kappa_0)$.
(2) Transport in the inertial subrange from κ_0 to the velocity-dissipation wavenumber $\kappa_U = C_U^{3/2}\kappa_K$ represented by n_2 substages with upper-cutoff wavenumbers,

$$\kappa_{2,j} = \left(\frac{3^j}{C_U Re_1 + 3^j - 1}\right)^{3/2}\kappa_U = f_{2,j}\kappa_U, \tag{14}$$

and $\kappa_{2,n_2} = \kappa_U$. In fully developed turbulence,[34] $C_U \approx 0.125 = C_D/2$ so that $\kappa_U \approx \kappa_K/22.6$.

(3) Transport in the viscous-convective subrange $(1<Sc)$ from κ_U to $\kappa_\phi = Sc^{1/2}\kappa_U$ represented by n_3 substages with upper-cutoff wavenumbers $\kappa_{3,j} = Sc^{j/(2n_3)}\kappa_U$.

The scalar energy at wavenumbers above κ_ϕ will be denoted by $\langle \phi_D'^2\rangle$ and can be found by subtraction:

$$\langle \phi_D'^2\rangle = \langle \phi'^2\rangle - \langle \phi_1'^2\rangle - \langle \phi_{2,1}'^2\rangle - \cdots - \langle \phi_{2,n_2}'^2\rangle - \langle \phi_{3,1}'^2\rangle - \cdots - \langle \phi_{3,n_3}'^2\rangle. \tag{15}$$

By assumption, all scalar dissipation occurs at wavenumbers above κ_ϕ; thus,

$$\frac{D\langle \phi_D'^2\rangle}{Dt} = 2T_D - 2\langle \epsilon_\phi\rangle. \tag{16}$$

However, this expression is redundant since Eqs. (2), (15) and the SR model provide a complete description of the scalar energy distribution.

The SR model for $1<Sc$ and $1<C_U Re_1$ is given by

$$\frac{D\langle \phi_1'^2\rangle}{Dt} = 2T_1 + 2\gamma_1 S_{\phi^2}, \tag{17}$$

$$\frac{D\langle \phi_{2,1}'^2\rangle}{Dt} = 2T_{2,1} + 2\gamma_{2,1} S_{\phi^2}, \tag{18}$$

$$\vdots$$

$$\frac{D\langle \phi_{2,n_2}'^2\rangle}{Dt} = 2T_{2,n_2} + 2\gamma_{2,n_2} S_{\phi^2}, \tag{19}$$

$$\frac{D\langle \phi_{3,1}'^2\rangle}{Dt} = 2T_{3,1} + 2\gamma_D S_{\phi^2}, \tag{20}$$

$$\frac{D\langle \phi_{3,2}'^2\rangle}{Dt} = 2T_{3,2}, \tag{21}$$

$$\vdots$$

$$\frac{D\langle \phi_{3,n_3}'^2\rangle}{Dt} = 2T_{3,n_3}, \tag{22}$$

and

$$\frac{D\langle \epsilon_\phi\rangle}{Dt} = 2C_D Re_1\langle\omega\rangle T_D + 2C_s Re_1\langle\omega\rangle\langle\epsilon_\phi\rangle - 2C_d\langle r_\phi\rangle_o\langle\epsilon_\phi\rangle, \tag{23}$$

where $\langle r_\phi\rangle_o$ is defined by

$$\langle r_\phi\rangle_o = C_D Re_1\langle\omega\rangle(1-\langle\varsigma_D\rangle) + \langle r_\phi\rangle. \tag{24}$$

For the case $Sc=1$, $n_3=0$ and the source term in Eq. (20) is added to the right-hand side of Eq. (16). In addition, Eq. (23) becomes

$$\frac{D\langle \epsilon_\phi\rangle}{Dt} = 2C_D Re_1\langle\omega\rangle T_D + 2C_D Re_1\langle\omega\rangle\gamma_D S_{\phi^2} + 2C_s Re_1\langle\omega\rangle\langle\epsilon_\phi\rangle - 2C_d\langle r_\phi\rangle_o\langle\epsilon_\phi\rangle. \tag{25}$$

The source weights, $0\leqslant\gamma_{i,j}\leqslant 1$, sum to unity and are further discussed below.

In the SR model, the spectral transport terms that model the energy cascade from large to small scales have the following forms:

$$T_1 = -\alpha_1\langle \phi_1'^2\rangle - \beta_1\langle \phi_1'^2\rangle + \beta_{2,1}\langle \phi_{2,1}'^2\rangle, \tag{26}$$

$$T_{2,1} = \alpha_1\langle \phi_1'^2\rangle - \alpha_{2,1}\langle \phi_{2,1}'^2\rangle + \beta_1\langle \phi_1'^2\rangle - 2\beta_{2,1}\langle \phi_{2,1}'^2\rangle + \beta_{2,2}\langle \phi_{2,2}'^2\rangle, \tag{27}$$

$$\vdots$$

$$T_{2,n_2} = \alpha_{2,n_2-1}\langle \phi_{2,n_2-1}'^2\rangle - \alpha_{2,n_2}\langle \phi_{2,n_2}'^2\rangle + \beta_{2,n_2-1}\langle \phi_{2,n_2-1}'^2\rangle - 2\beta_{2,n_2}\langle \phi_{2,n_2}'^2\rangle + \beta_{3,1}\langle \phi_{3,1}'^2\rangle, \tag{28}$$

$$T_{3,1} = \alpha_{2,n_2}\langle \phi_{2,n_2}'^2\rangle - \alpha_{3,1}\langle \phi_{3,1}'^2\rangle + \beta_{2,n_2}\langle \phi_{2,n_2}'^2\rangle - 2\beta_3\langle \phi_{3,1}'^2\rangle + \beta_3\langle \phi_{3,2}'^2\rangle, \tag{29}$$

$$\vdots$$

$$T_{3,n_3} = \alpha_3\langle \phi_{3,n_3-1}'^2\rangle - \alpha_3\langle \phi_{3,n_3}'^2\rangle + \beta_3\langle \phi_{3,n_3-1}'^2\rangle - 2\beta_3\langle \phi_{3,n_3}'^2\rangle + \beta_D\langle \phi_D'^2\rangle, \tag{30}$$

and

$$T_D=\alpha_3\langle\phi'^2_{3,n_3}\rangle+\beta_3\langle\phi'^2_{3,n_3}\rangle-\beta_D\langle\phi'^2_D\rangle. \tag{31}$$

Note that the sum of the spectral transport terms is null, thereby conserving scalar energy as it moves through wavenumber space.

The SR model rate coefficients $\alpha_{i,j}$ and $\beta_{i,j}$ represent the rates of convective and diffusive transport, respectively, along the scalar spectrum. Only the case where $\beta_{i,j}=0$ has been considered in detail.[4] For this case, the rate coefficients $\alpha_{i,j}=t_{i,j}^{-1}$ follow directly from the fully developed turbulent velocity spectrum:[4]

$$t_1=\frac{1}{\langle\omega\rangle}, \tag{32}$$

$$t_{2,1}=\left(1-\frac{1}{C_URe_1}\right)t_1, \tag{33}$$

$$t_{2,j}=\frac{1}{3}t_{2,j-1}, \tag{34}$$

$$t_{2,n_2-1}=\frac{1}{3}t_{2,n_2-2}, \tag{35}$$

$$t_{2,n_2}=\frac{1}{2}t_{2,n_2-1}, \tag{36}$$

$$t_3=\frac{\ln(Sc)}{2n_3Re_1}t_1. \tag{37}$$

The values of n_2 ($2\leqslant n_2$) and n_3 ($0\leqslant n_3$) increase linearly with $\ln(Re_1)$ and $\ln(Sc)$, respectively.[4] Choosing n_2 and n_3 larger than their minimum values will not adversely affect the SR model's predictions since the excess stages will quickly relax to (quasi) steady-state values. Note that t_1, the characteristic time scale of the energy-containing range of the velocity spectrum, is a key parameter in the model (e.g., it determines the spectral flux at large scales and the scalar dissipation rate at spectral equilibrium), and is dependent on the form of the velocity spectrum at large scales. The SR model could thus be further refined by including a more detailed description of the large scales using, for example, large-eddy simulation (LES).

The rate coefficients for the convective-diffusive case ($0<\beta_{i,j}$) can be derived, for example, from the spectral transport model of Leith[35] in the form proposed by Besnard *et al.*[36,37] The primary difference with the convective case ($\beta_{i,j}=0$) is the allowance for scalar-energy transport from small to large scales. Without this ''reverse'' transport, the steady-state value of $\langle r_\phi\rangle$ may depend on the initial scalar spectrum in the absence of a mean scalar gradient[4] (e.g., if $\langle\phi'^2_1\rangle=0$ at $t=0$ it will remain so for all time, in which case, if $0<\langle\phi'^2_{2,1}\rangle$, $\langle r_\phi\rangle\rightarrow 2t_1/t_{2,1}$). For inhomogeneous flows, mean scalar gradients produce scalar energy at large scales ($0<\gamma_1 S_{\phi^2}$) and ''forward'' transport dominates. Thus, the differences found by neglecting the diffusive terms may be negligible for many practical applications.

In the SR model, the source weights ($\gamma_{i,j}$) are specified by forcing the self-similar scalar spectrum for the case $Sc=1$ ($n_3=0$) to be the same for all values of S_{ϕ^2}. This condition yields

$$\langle\omega\rangle=\lim_{t\rightarrow\infty}\langle r_\phi\rangle \text{ and } \gamma_{i,j}=\lim_{t\rightarrow\infty}\langle s_{i,j}\rangle,$$

$$\text{with } Sc=1 \text{ and } S_{\phi^2}=0, \tag{38}$$

and

$$\gamma_D=1-\gamma_1-\sum_{j=1,n_2}\gamma_{2,j}=\frac{1}{C_DRe_1}. \tag{39}$$

For example, for the convective case with $n_2=3$, the source weights are easily found to be

$$\gamma_1=b(1-a)(1-a/6)(1-a/3), \tag{40}$$

$$\gamma_{2,1}=ab(1-a/6)(1-a/3), \tag{41}$$

$$\gamma_{2,2}=ab(1-a/6)/3, \tag{42}$$

$$\gamma_{2,3}=ab/6, \tag{43}$$

$$\gamma_D=1-b, \tag{44}$$

where

$$a=1-\frac{1}{C_URe_1}$$

and

$$b=1-\frac{1}{C_DRe_1}.$$

Note that as $Re_1\rightarrow\infty$, a and $b\rightarrow 1$ yielding $\gamma_1=\gamma_D=0$ and implying that almost all of the scalar energy will be contained in the wavenumber range $[\kappa_0,\kappa_\phi]$ at very high Reynolds numbers.

As noted in the Introduction, the SR model as given above differs slightly from the original version.[4] The main differences are the introduction of the source weights ($\gamma_{i,j}$), the effective scalar-field dimension N_z, and the velocity-dissipation constant C_U (in the original model $\gamma_{2,1}=N_z=C_U=1$). These changes result in very minor differences in the model predictions. For example, the case of stationary turbulence with $Sc=1$ yields a limiting mechanical-to-scalar time-scale ratio of

$$\langle r\rangle=\frac{2\langle r_\phi\rangle}{\langle\omega\rangle}=2, \tag{45}$$

which agrees with the original model for large R_λ. Finally, since the dynamical behavior of the SR model is mainly influenced by the relaxation of the large scales, the conclusions drawn concerning its ability to correctly handle scalar mixing in decaying turbulence are equally valid for the new version.

III. LAGRANGIAN SPECTRAL RELAXATION MODEL

The SR model can be extended to inhomogeneous flows and solved using a standard finite-volume CFD code, thus providing a dynamic model for the *mean* scalar dissipation rate. However, for reacting flows the reaction source term would still be unclosed, leading to many well-known difficulties.[3] A powerful alternative approach is to employ Lagrangian pdf methods wherein the turbulent transport and reaction terms appear in closed form.[3] In this section, we

develop a Lagrangian pdf version of the spectral relaxation (LSR) model formulated in terms of a set of stochastic differential equations for the scalar spectral distribution and the scalar dissipation rate following a fluid particle. The validity of describing the spectral energy cascade by a Lagrangian approach has recently been demonstrated using DNS data,[38] and employed in a dynamic subgrid-scale model for LES.[39] In developing the LSR model, we follow the approach of Borgas and Sawford[40] and formulate the model in terms of a Markovian process conditioned on a particular *turbulent frequency* history $\mathscr{W}(t)=\{\omega^*(s)|s \in (-\infty,t]\}$ for each fluid particle, where $\omega^*(t)$ is defined by Eq. (49) below.

In Lagrangian pdf methods, the turbulent flow is represented by a large ensemble of fluid particles whose time evolution is approximated by stochastic models that are solved using Monte-Carlo methods. In a statistically homogeneous flow, the one-point statistics for the scalar field are everywhere identical; hence, the physical size of the fluid particle is unimportant. However, in the same flow, since any two points separated by more than the velocity-dissipation correlation length scale ($l_U \approx 22.6\eta$ based on $\kappa_U = C_U^{3/2}\kappa_K$) must necessarily have different strain-rate histories, conditioning on $\mathscr{W}$ must imply that the fluid particles have a linear dimension at least as small as l_U. Since a particle's scalar dissipation rate in the LSR model will depend on its particular $\mathscr{W}$, *conditional* one-point statistics (e.g., $\langle \phi'^2|\mathscr{W}\rangle$) will be inhomogeneous near the Kolmogorov scale, even though the flow is homogeneous on the integral scale. These small-scale inhomogeneities generate additional scale-dependent mixing terms (i.e., in addition to the uniform mean scalar gradient term) in the LSR model. Moreover, we shall also see that they generate an asymptotic non-Gaussian scalar pdf (i.e., although the conditional scalar pdf is Gaussian, the unconditional pdf need not be). Likewise, the initial scalar field may be inhomogeneous at some scales above the integral scale (e.g., ''blobs'' of fluid with different scalar spectra at wavenumbers smaller than κ_0). As demonstrated in a recent DNS study,[22] these ''non-equilibrium'' spectral effects can be a source of transient non-Gaussian statistics. This behavior is also captured by the LSR model.

Formally, we can define a Lagrangian fluid particle in terms of the Eulerian velocity field by introducing a compact spatial filter function $0 \leqslant K(\mathbf{x})$ with bandwidth proportional to l_U, and

$$\int_{\mathscr{V}} K(\mathbf{x})d\mathbf{x} = 1, \tag{46}$$

where $\mathscr{V}$ is the fluid volume. In terms of the filter, the fluid particle velocity becomes

$$\widetilde{U}_i(t) = \int_{\mathscr{V}} K(\mathbf{x}-\mathbf{x}^*)U_i(\mathbf{x},t)d\mathbf{x}, \tag{47}$$

where

$$\frac{dx_i^*}{dt} = \widetilde{U}_i \tag{48}$$

governs the fluid particle position. Likewise, the turbulent frequency following the fluid particle can be defined by[41,42]

$$\omega^*(t) = \omega(\mathbf{x}^*(t),t) = \frac{\epsilon(\mathbf{x}^*(t),t)}{\langle k\rangle}. \tag{49}$$

Note that since the velocity spectral energy below l_U is small compared to the total energy, the same Lagrangian pdf model can be employed for $\widetilde{U}_i(t)$ or $U_i^*(t) = U_i(\mathbf{x}^*(t),t)$. Hereinafter, we will thus denote the fluid particle velocity by U_i^*. Nevertheless, Kolmogorov-scale velocity fluctuations: $u_i' = U_i^* - \widetilde{U}_i \propto (\nu\langle\epsilon\rangle)^{1/4}$, while negligible relative to integral-scale fluctuations, are responsible for inter-particle transport of spectral energy, and therefore are included in the LSR model.

The LSR model is written in terms of conditional means of the form $\langle \phi_{i,j}'^2|\mathbf{u}^*,\mathscr{W}\rangle$. Theoretically, the unconditional expectations appearing in the SR model can be found by averaging over the velocity and the set $\mathscr{M}$ of all possible realizations of $\mathscr{W}$ weighted by the probability measure $dF_{\mathscr{W}}$,[43] i.e.,

$$\langle \phi'^2\rangle = \int_{\mathscr{M}} \langle \phi'^2|\mathscr{W}\rangle dF_{\mathscr{W}}. \tag{50}$$

Numerically, unconditional expectations are computed by generating a large number of independent samples of $\mathscr{W}$, and ensemble averaging the solutions to the LSR model. Hereinafter, in order to simplify the notation, we shall avoid introducing a specific notation for velocity, $\mathscr{W}$-conditional expectations and simply let, for example,

$$\langle \phi'^2\rangle^* = \langle \phi'^2|\mathbf{u}^*,\mathscr{W}\rangle. \tag{51}$$

However, this simplification will be avoided when it may cause confusion. For example, when computing the scalar pdf, it will be necessary to introduce the random process $\phi'^*(t) = \phi'(\mathbf{x}^*(t),t)$, and to model conditional expectations of the form $\langle \Gamma\nabla^2\phi'|\phi'^*,\mathbf{u}^*,\mathscr{W}\rangle$. Furthermore, due to the numerical difficulties associated with estimating velocity-conditioned scalar statistics,[44] the LSR model will be presented in a velocity-independent form so that hereinafter the notation $\langle\cdot\rangle^*$ will denote only the $\mathscr{W}$-conditioned expectation, e.g.,

$$\langle \phi'^2\rangle^* = \langle \phi'^2|\mathscr{W}\rangle. \tag{52}$$

Nevertheless, a velocity-conditioned formulation of the model can be derived by substituting velocity-conditioned scalar statistics for unconditional ones, e.g., $\langle \phi_1'^2\rangle$ becomes $\langle \phi_1'^2|\mathbf{u}^*\rangle$ and $\langle \phi_1'^2\rangle^*$ is given by Eq. (51).

When applying the LSR model, the reader should be careful to distinguish $\langle \phi'^2\rangle^*$ from $\langle \phi'^2|\omega^*\rangle$, i.e., the scalar variance conditioned on $\mathscr{W}$ from the scalar variance conditioned on the current value of ω^*. At any instant, many spatially uncorrelated points in a given flow will have nearly identical ω^*; however, only points separated by approximately l_U i.e., inside a fluid particle) can have nearly identical $\mathscr{W}$. Likewise, it is important to distinguish between the random variables $\epsilon_\phi^*(t) = \epsilon_\phi(\mathbf{x}^*(t),t)$ and $\langle\epsilon_\phi\rangle^*$. The latter will have a single value for each fluid particle, while the former will vary randomly inside each fluid particle [e.g., consider $1 \ll Sc$ where the fine-scale structure of the scalar dissipation field ($l_D \approx 0.35 l_U/Sc^{1/2}$) is much smaller than

l_U]. Hence, $\langle \epsilon_\phi \rangle^*$ corresponds to the expectation of ϵ_ϕ^* inside of a fluid particle. It is thus useful to decompose ϵ_ϕ^* into the product of two terms:

$$\epsilon_\phi^* = \langle \epsilon_\phi \rangle^* Z^2, \tag{53}$$

where $Z(t)$ is a standardized random process that contains the effect of molecular diffusion on the scalar gradient pdf, and $\langle \epsilon_\phi \rangle^*$ models the effects of turbulence and molecular dissipation on the scalar microscale. For large Sc, separation of scales can be invoked to argue that Z and $\langle \epsilon_\phi \rangle^*$ will be independent random processes if time is rescaled:

$$dt^\dagger = \omega_\phi^\dagger \, dt, \tag{54}$$

using the ''local'' scalar dissipation rate:

$$\omega_\phi^\dagger = \frac{\langle \epsilon_\phi \rangle^*}{\langle \phi'^2 \rangle^*}. \tag{55}$$

This is the approach taken by Fox[20] where a model is proposed for the standardized scalar (V) and scalar gradient (Z) for the special case where $\omega^* = \langle \omega \rangle$ (i.e., all fluid particles have identical strain-rate histories so that $\omega_\phi^\dagger = \langle r_\phi \rangle$).

The remainder of this section is organized as follows. First, Lagrangian pdf models for the velocity and turbulent frequency are reviewed and a new model for the latter is proposed that more closely reproduces the one-point statistics of $\omega(\mathbf{x},t)$ found in the DNS study of Overholt and Pope.[21] Next, the LSR model equations are presented for the convective transport case ($\beta_{i,j} = 0$). Finally, models for conditional molecular mixing and the conditional turbulent scalar flux terms are introduced to describe the evolution of the scalar and scalar gradient in a fluid particle. A detailed comparison between model predictions and DNS data for passive scalar mixing in stationary, isotropic turbulence is presented in the Sec. IV.

A. Lagrangian pdf models for the velocity and turbulent frequency

Pope and co-workers[12] have used Lagrangian pdf methods to derive and verify stochastic models based on the Langevin equation to describe the position, velocity, and turbulent frequency of a fluid particle in a turbulent flow. In these models, the fluid-particle velocity and turbulent frequency are denoted by U_i^* and ω^*, respectively, and obey

$$dU_i^* = -\frac{1}{\rho}\frac{\partial \langle p \rangle}{\partial x_i} dt + L_{i,j}(U_j^* - \langle U_j \rangle) dt + (C_0 \langle k \rangle \omega^*)^{1/2} \, dW_i \tag{56}$$

and

$$d\omega^* = -\omega^* \langle \omega \rangle \left[S_\omega + C_\chi \left(\ln\left(\frac{\omega^*}{\langle \omega \rangle} \right) - \left\langle \frac{\omega}{\langle \omega \rangle} \ln\left(\frac{\omega}{\langle \omega \rangle} \right) \right\rangle \right) \right] dt + \langle \omega \rangle^2 h \, dt + \omega^* (2 C_\chi \langle \omega \rangle \sigma^2)^{1/2} \, dW_\omega. \tag{57}$$

The parameters and coefficients appearing on the right-hand sides above are described in detail elsewhere.[12] Note that the mean fields are evaluated at x^* and thus the coefficients depend on both time and location in inhomogeneous flows. For all fluid-particle variables, the models are constructed such that the Lagrangian expectations obey an equivalent Reynolds-stress model.[45] In a homogeneous flow, Eq. (56) generates a multi-variate Gaussian velocity field and Eq. (57), an independent log-normal turbulent frequency field.

In statistically homogeneous flows, Eq. (57) is self-contained (coefficients are independent of x^*) and the term involving h needed to generate non-zero turbulent frequency in fluid particles with $\omega^* = 0$, but which are located in a turbulent region of the flow: $0 < \langle \omega \rangle$, is null. It has been noted[40] that this model for ω^* does not yield the expected highly intermittent behavior of turbulent dissipation at very high Reynolds number. More importantly, in the DNS study[21] that will be employed for model validation, the turbulent frequency pdf is not well represented by a log-normal pdf, but instead has a stretched-exponential tail whose decay exponent depends on the turbulent Reynolds number. Since the one-point, one-time statistics computed from the LSR model are sensitive to the modeled turbulent-frequency pdf, we shall employ the following model that more closely approximates the observed pdf:

$$d\omega^* = -\omega^* \langle \omega \rangle S_\omega dt + \omega^* \langle \omega \rangle C_\chi Re_1 \times \left(1 - \frac{(\omega^*)^{\gamma_{\omega 1}} \langle \omega \rangle}{\langle \omega^{\gamma_{\omega 1}+1} \rangle} \right) dt + \langle \omega \rangle^2 h \, dt + \omega^* \left(\frac{2 C_\chi Re_1 \langle \omega \rangle}{\gamma_{\omega 2}} \right)^{1/2} dW_\omega, \tag{58}$$

where $\gamma_{\omega 1}$ and $\gamma_{\omega 2}$ are model parameters that depend on ω^* and Re_1 as discussed below, and C_χ controls the autocorrelation time of the random process $\omega^*(t)$. Note, however, that the limiting form of the turbulent frequency pdf does not uniquely determine the model. For example, the same limiting pdf could be obtained by replacing the second term of the right-hand side of Eq. (58) with

$$\langle \omega \rangle^2 C_\chi Re_1 \left(1 - \frac{(\omega^*)^{\gamma_{\omega 1}}}{\langle \omega^{\gamma_{\omega 1}} \rangle} \right),$$

and the noise-term coefficient with

$$\left(\frac{2 C_\chi Re_1 \langle \omega \rangle \omega^*}{\gamma_{\omega 2} - 1} \right)^{1/2}.$$

Defining $X = \omega^*/\langle \omega \rangle$, in homogeneous turbulence the limiting pdf resulting from Eq. (58) with *constant* parameters is

$$f_X(x) = \mathcal{N} x^{\gamma_{\omega 2} - 2} \exp\left(-\frac{\gamma_{\omega 2}}{\gamma_{\omega 1}} \frac{x^{\gamma_{\omega 1}}}{\langle X^{\gamma_{\omega 1}+1} \rangle} \right), \tag{59}$$

where $\mathcal{N}$ is a normalization constant. Fitting this function to the pdf found by DNS[21] yields

$$\lim_{X \to 0} \gamma_{\omega 2} = 3.33, \tag{60}$$

$$\lim_{X \to \infty} \gamma_{\omega 2} = 1.5, \tag{61}$$

and $\gamma_{\omega 1}$ is a function of Re_1 (e.g., for $Re_1=10.72$, $\gamma_{\omega 1}=0.778$, and for $Re_1=32.38$, $\gamma_{\omega 1}=0.500$). We will thus let

$$\gamma_{\omega 2}=\frac{3.33+1.5C_\omega X}{1+C_\omega X}, \tag{62}$$

and fix $C_\omega=0.35$ by forcing $\langle X^2\rangle$ to agree with the DNS data (Sec. IV).

Note that the auto-correlation time predicted by Eq. (58) will scale like $1/(C_\chi Re_1\langle\omega\rangle)$, i.e., it does not reproduce the small-scale intermittency expected at large Reynolds numbers.[40,46] Moreover, although the auto-correlation time can be varied by changing C_χ, $\omega^*(t)$ still remains Markovian contrary to the requirements of small-scale intermittency.[40,46] Thus, in order to test its importance in determining the scalar statistics in the LSR model, numerical studies with C_χ significantly larger and smaller than unity have been carried out. In general, the effect of the auto-correlation time on the one-point statistics of the scalar dissipation has been found to be small compared to the effect of the form of stationary turbulent-frequency pdf. On the other hand, when the auto-correlation time decreases, the correlation between ω^* and the scalar dissipation also decreases. This limiting behavior is consistent with the ''white-noise'' models for the vortex-stretching term employed in other studies.[47,48] We therefore conclude that, although it does not correctly reproduce small-scale intermittency, Eq. (58) should suffice for a quantitative comparison with the DNS data.

B. Lagrangian pdf model for the conditional means

The LSR model (convective case) for $1<Sc$ and $1<C_U Re_1$ ($Sc=1$ is handled as in the SR model) is given by

$$\frac{d\langle\phi_1'^2\rangle^*}{dt}=-2\alpha_1\langle\phi_1'^2\rangle^*+2f_D\langle r_\phi\rangle(\langle\phi_1'^2\rangle-\langle\phi_1'^2\rangle^*)+2\gamma_1 S_{\phi^2}, \tag{63}$$

$$\frac{d\langle\phi_{2,1}'^2\rangle^*}{dt}=2\alpha_1(f_1\langle\phi_1'^2\rangle^*+f_1^c\langle\phi_1'^2\rangle)-2\alpha_{2,1}\langle\phi_{2,1}'^2\rangle^*+2f_D\langle r_\phi\rangle(\langle\phi_{2,1}'^2\rangle-\langle\phi_{2,1}'^2\rangle^*)+2\gamma_{2,1}S_{\phi^2}, \tag{64}$$

$$\vdots$$

$$\frac{d\langle\phi_{2,n_2}'^2\rangle^*}{dt}=2\alpha_{2,n_2-1}(f_{2,n_2-1}\langle\phi_{2,n_2-1}'^2\rangle^*+f_{2,n_2-1}^c\langle\phi_{2,n_2-1}'^2\rangle)-2\alpha_{2,n_2}\langle\phi_{2,n_2}'^2\rangle^*+2f_D\langle r_\phi\rangle(\langle\phi_{2,n_2}'^2\rangle-\langle\phi_{2,n_2}'^2\rangle^*)+2\gamma_{2,n_2}S_{\phi^2}, \tag{65}$$

$$\frac{d\langle\phi_{3,1}'^2\rangle^*}{dt}=2\alpha_{2,n_2}(f_{2,n_2}\langle\phi_{2,n_2}'^2\rangle^*+f_{2,n_2}^c\langle\phi_{2,n_2}'^2\rangle)-2\alpha_3\sigma(t)\langle\phi_{3,1}'^2\rangle^*+2f_D\langle r_\phi\rangle(\langle\phi_{3,1}'^2\rangle-\langle\phi_{3,1}'^2\rangle^*)+2\gamma_D S_{\phi^2}, \tag{66}$$

$$\frac{d\langle\phi_{3,2}'^2\rangle^*}{dt}=2\alpha_3\sigma(t)\langle\phi_{3,1}'^2\rangle^*-2\alpha_3\sigma(t)\langle\phi_{3,2}'^2\rangle^*+2f_D\langle r_\phi\rangle(\langle\phi_{3,2}'^2\rangle-\langle\phi_{3,2}'^2\rangle^*), \tag{67}$$

$$\vdots$$

$$\frac{d\langle\phi_{3,n_3}'^2\rangle^*}{dt}=2\alpha_3\sigma(t)\langle\phi_{3,n_3-1}'^2\rangle^*-2\alpha_3\sigma(t)\langle\phi_{3,n_3}'^2\rangle^*+2f_D\langle r_\phi\rangle(\langle\phi_{3,n_3}'^2\rangle-\langle\phi_{3,n_3\prime 2}\rangle^*), \tag{68}$$

$$\frac{d\langle\phi_D'^2\rangle^*}{dt}=2\alpha_3\sigma(t)\langle\phi_{3,n_3}'^2\rangle^*+2f_D\langle r_\phi\rangle(\langle\phi_D'^2\rangle-\langle\phi_D'^2\rangle^*)-2\langle\epsilon_\phi\rangle^*, \tag{69}$$

and

$$\frac{d\langle\epsilon_\phi\rangle^*}{dt}=2C_D Re_1\langle\omega\rangle\alpha_3\sigma(t)\langle\phi_{3,n_3}'^2\rangle^*+2f_D\langle r_\phi\rangle(\langle\epsilon_\phi\rangle-\langle\epsilon_\phi\rangle^*)+2C_s Re_1\langle\omega\rangle\sigma(t)\langle\epsilon_\phi\rangle^*-2C_d\langle r_\phi\rangle_o^\dagger\langle\epsilon_\phi\rangle^*, \tag{70}$$

where $f_1=\kappa_0/\kappa_U=(C_U Re_1)^{-3/2}$, $f_1^c=1-f_1$, $f_{2,j}=\kappa_{2,j}/\kappa_U$, $f_{2,j}^c=1-f_{2,j}$,

$$\langle r_\phi\rangle_o^\dagger=C_D Re_1\langle\omega\rangle(1-\langle\varsigma_D\rangle^\dagger)+\omega_\phi^\dagger, \tag{71}$$

$$\langle\varsigma_D\rangle^\dagger=\frac{\langle\phi_D'^2\rangle^*}{\langle\phi'^2\rangle^*}, \tag{72}$$

and

$$\sigma(t)=\left(\frac{\omega^*}{\langle\omega\rangle}\right)^{1/2}. \tag{73}$$

Note that the LSR model contains no independent ''noise'' term: all fluctuations are generated by ω^* in Eq. (73). This results from the assumption that the random scalar-gradient-amplification, ''vortex-stretching'' events in the dissipation range of the velocity spectrum have a Lagrangian time history of the form

$$\left\langle\Gamma\frac{\partial\phi'}{\partial x_i}\frac{\partial u_j}{\partial x_i}\frac{\partial\phi'}{\partial x_j}\middle|\mathscr{W}\right\rangle=-C_s\left(\frac{\epsilon^*}{\nu}\right)^{1/2}\langle\epsilon_\phi\rangle^*. \tag{74}$$

This model is supported by DNS[49,50] and experimental[51,52] studies of the scalar gradient alignment in isotropic and sheared turbulence where it is found that the scalar gradient is preferentially aligned in the direction opposite the eigenvector of the most compressive principal strain rate, ϵ_{11}. In a solenoidal flow, ϵ^* can be expressed in terms of ϵ_{11} as[52]

$$\epsilon^*=4\nu\epsilon_{11}^2(1+\delta+\delta^2), \tag{75}$$

where $-1/2\leqslant\delta\leqslant 1$ is the ratio of the intermediate and the most compressive principal strain rates. The pdf of δ has a strong peak at the origin;[50,52] thus, letting $\delta=0$ and assuming that the scalar gradient is exactly colinear with the eigenvector (implying $N_z=1$) yields Eq. (74) with $C_s=0.5$.

As in the SR model, Eq. (69) can be replaced by an expression for $\langle\phi'^2\rangle^*$ found by summing Eqs. (63)–(69):

$$\frac{d\langle\phi'^2\rangle^*}{dt}=2S_{\phi^2}+\mathscr{T}_\phi+\mathscr{D}_\phi-2\langle\epsilon_\phi\rangle^*. \tag{76}$$

The inertial-range mixing term, defined by

$$\mathscr{T}_\phi=2\alpha_1 f_1^c(\langle\phi_1'^2\rangle-\langle\phi_1'^2\rangle^*)+\cdots +2\alpha_{2,n_2}f_{2,n_2}^c(\langle\phi_{2,n_2}'^2\rangle-\langle\phi_{2,n_2}'^2\rangle^*), \tag{77}$$

is a model for the dissipation of large-scale scalar field inhomogeneities by the velocity field:

$$\left\langle u_i\frac{\partial\phi'^2}{\partial x_i}\middle|\mathscr{W}^*\right\rangle=-\mathscr{T}_\phi. \tag{78}$$

While the diffusive-mixing term, defined by

$$\mathscr{D}_\phi=2f_D\langle r_\phi\rangle(\langle\phi'^2\rangle-\langle\phi'^2\rangle^*), \tag{79}$$

is a model for the molecular dissipation of small-scale scalar variance inhomogeneities generated by the difference in the scalar dissipation rate between any two fluid particles:

$$\langle\Gamma\nabla^2\phi'^2|\mathscr{W}^*\rangle=\mathscr{D}_\phi. \tag{80}$$

The scalar-variance source term, being the product of two integral-scale fields, is assumed to be independent of $\mathscr{W}^*$, i.e., $\langle u_i\phi'|\mathscr{W}^*\rangle=\langle u_i\phi'\rangle$. Note that for the case of a statistically homogeneous scalar field with $\omega^*=\langle\omega\rangle$, $\mathscr{T}_\phi=\mathscr{D}_\phi=0$ and $\langle\epsilon_\phi\rangle^*=\langle\epsilon_\phi\rangle$; hence, $\langle\phi'^2\rangle^*=\langle\phi'^2\rangle$ and $\omega_\phi^\dagger=\langle r_\phi\rangle$. The LSR model thus reverts to the ''standard'' model for statistically homogeneous scalar mixing when turbulent frequency fluctuations are ignored.

In general, the physical significance of each term in the LSR model follows from the analogous term in the SR model. Terms that drop out in the SR model [e.g., $f_D\langle r_\phi\rangle\times(\langle\phi_1'^2\rangle-\langle\phi_1'^2\rangle^*)$] are needed to model flows that are inhomogeneous at some scale as noted above. The same remark applies for the use of the weighted unconditional means in the first terms on the right-hand sides of Eqs. (64)–(66). The weights, $f_{i,j}=$(particle size)/(wavelength of inhomogeneity), represent the influence of a single particle on the mean of all particles within a diameter of one wavelength around the fluid particle. Note that in a statistically homogeneous flow with all particles having the same initial conditions, Eqs. (63)–(65) yield $\langle\phi_1'^2\rangle=\langle\phi_1'^2\rangle^*$ and $\langle\phi_{2,j}'^2\rangle=\langle\phi_{2,j}'^2\rangle^*$. This is a result of the model assumption that random vortex-stretching events are significant only at wavenumbers above the velocity-dissipation wavenumber κ_U. Above κ_U, convective spectral transport occurs only within a fluid particle, and thus the first terms on the right-hand sides of Eqs. (67)–(69) contain the conditional means. Also note that the molecular dissipation term in Eq. (70) employs the ''local'' scalar dissipation rate $\omega_\phi^\dagger$. This reflects the fact that molecular diffusion occurs on small scales that adjust to local, as opposed to global, flow conditions.

Finally, note that fluctuations due to $\sigma(t)$ in Eqs. (66)–(70) will generate inhomogeneities below the velocity-dissipation scale which are dissipated by the diffusive-mixing terms, e.g.,

$$f_D\langle r_\phi\rangle(\langle\phi_{3,j}'^2\rangle-\langle\phi_{3,j}'^2\rangle^*).$$

The diffusive-mixing parameter f_D thus has a significant effect on the statistics of the ''local'' scalar-variance ratio defined by

$$\Phi=\frac{\langle\phi'^2\rangle^*}{\langle\phi'^2\rangle}. \tag{81}$$

This can most easily be seen from the governing expression for Φ for the case $S_{\phi^2}=\mathscr{T}_\phi=0$:

$$\frac{d\Phi}{dt}=2f_D\langle r_\phi\rangle-2[\langle r_\phi\rangle(f_D-1)+\omega_\phi^\dagger]\Phi. \tag{82}$$

When $f_D=1$, the eigenvalue of Eq. (82) is $-2\omega_\phi^\dagger\leqslant 0$, and thus the equation is unconditionally stable. On the other hand, when $f_D=0$ the eigenvalue is $-2(\omega_\phi^\dagger-\langle r_\phi\rangle)$, and thus it fluctuates between positive and negative values. Hence, Eq. (82) is stochastically unstable (e.g., when $\omega_\phi^\dagger<\langle r_\phi\rangle$ for all t), and the moments $\langle\Phi^n\rangle$, $1<n$ can grow unbounded. The resulting large variations in Φ will generate strongly non-Gaussian scalar pdfs. It is also worth noting that instability is not observed in the presence of a uniform mean scalar gradient ($0<S_{\phi^2}$), and thus the predicted scalar pdf will be closer to Gaussian for all values of f_D. This result agrees with DNS[22] where significant non-Gaussian tails are seen only in the absence of a uniform mean scalar gradient.

C. Molecular mixing

The LSR model provides a closure for the (conditional) scalar dissipation rate following a Kolmogorov-scale fluid particle. However, it provides no information concerning fluctuations of the scalar and scalar dissipation *inside* the fluid particle (ϕ'^* and ϵ_ϕ^*, respectively) resulting from molecular diffusion (the so-called molecular mixing term[19,20]). Due to the sensitive dependence of the joint scalar, scalar gradient pdf on the initial scalar field, development of completely general molecular mixing models remains an open problem.[19,20,53–55] For binary mixing of an inert scalar, Fox[20] proposed the Fokker–Planck model and obtained satisfactory agreement with data from the numerical solution of the 1-D diffusion equation where, in the limit of large time, molecular mixing of an inert scalar by itself leads to independent joint Gaussian statistics for the scalar and scalar gradient. In this limit, the Fokker–Planck model reduces to a linear Fokker–Planck equation with coefficients conditioned on the ''local'' scalar dissipation rate [Eq. (54)], or, equivalently, on $\mathscr{W}^*$. The conditional scalar pdf then remains Gaussian with zero mean and variance $\langle\phi'^2|\mathscr{W}^*\rangle$, while the scalar dissipation is given by Eq. (53) with Z an independent, standard Gaussian random process.

From a modeling standpoint, the key assumption in developing $\mathscr{W}^*$-conditioned molecular mixing models is that after time rescaling [Eq. (54)], the model will be *independent* of the underlying velocity field. The model should thus depend only of the scalar field, and be equally applicable to cases with or without turbulence. Molecular mixing models can then be validated against numerical simulations of reactive-diffusive systems, or systems with a constant strain rate ($\mathscr{W}^*$ constant). (The initial length-scale distribution of

the scalar field should be ''non-singular'' to avoid degenerate cases.[19]) Note that this assumption does not exclude the difficulties resulting from initial conditions, unequal molecular diffusivities, or chemical reactions. However, it does place strong conditions on the model for the scalar gradients since they must agree with the non-trivial pdf found for pure diffusion.[20] Indeed, even for inert scalars, the scalar gradient pdf is strongly dependent of the initial scalar field (e.g., binary mixing[20] versus ternary mixing[56]) and bounded above by a ''diffusion-layer'' envelope[20] that is not accounted for in most scalar-gradient models.[48]

In the present study, the difficulty of closing the molecular mixing term will be circumvented by limiting consideration to an initial scalar field that is ''locally'' (i.e., in each fluid particle) Gaussian evolving in homogeneous turbulence with possibly a uniform mean scalar gradient.[44,57,58] The Lagrangian pdf equation for the scalar then simplifies to

$$\frac{d\phi'^*}{dt} = -\langle u_i | \phi'^*, \mathscr{W}\rangle \frac{\partial\langle\phi\rangle}{\partial x_i} - \left\langle u_i \frac{\partial\phi'}{\partial x_i} \middle| \phi'^*, \mathscr{W}\right\rangle + \langle \Gamma\nabla^2\phi' | \phi'^*, \mathscr{W}\rangle, \tag{83}$$

where the first two terms on the right-hand side arise from the turbulent scalar flux of the mean and fluctuating scalar gradient, respectively, and the third term is due to molecular mixing. Note that if all three terms are linear in ϕ'^*, the ''local'' ($\mathscr{W}$-conditioned) scalar field will remain Gaussian with variance $\langle\phi'^2|\mathscr{W}\rangle$; however, the ''global'' scalar pdf may be non-Gaussian due to the dependence on $\mathscr{W}$.

The conditional molecular mixing term for a Gaussian scalar field can be modeled by modifying the IEM model[3] to be consistent with the LSR model:

$$\langle \Gamma\nabla^2\phi' | \phi'^*, \mathscr{W}\rangle = -[\omega_\phi^\dagger + f_D\langle r_\phi\rangle(1-\Phi^{-1})]\phi'^*, \tag{84}$$

or by employing a modified limiting form of the Fokker–Planck model:[20]

$$\langle \Gamma\nabla^2\phi' | \phi'^*, \mathscr{W}\rangle dt = -[2\omega_\phi^\dagger + f_D\langle r_\phi\rangle \times(1-\Phi^{-1})]\phi'^*\, dt + (2\langle\epsilon_\phi\rangle^*)^{1/2}\, dW_\phi. \tag{85}$$

Note that both models, when written in terms of $t^\dagger$ [Eq. (54)] and the ''local'' standardized scalar field:

$$V = \frac{\phi'^*}{\sqrt{\langle\phi'^2\rangle^*}}, \tag{86}$$

are independent of $\mathscr{W}$. Likewise, both models yield the same $\mathscr{W}$-conditioned scalar-variance diffusion term:

$$2\langle\phi'\Gamma\nabla^2\phi' | \mathscr{W}\rangle = \mathscr{D}_\phi - 2\langle\epsilon_\phi\rangle^*, \tag{87}$$

which is consistent with Eq. (76). Direct comparison of these molecular mixing models with DNS data is challenging due to the difficulty of computing $\mathscr{W}$-conditioned scalar statistics. Thus, instead, we will compute the conditional scalar Laplacian:

$$\langle \Gamma\nabla^2\phi' | \phi'^*\rangle = -[\langle\omega_\phi^\dagger|\phi'^*\rangle + f_D\langle r_\phi\rangle \times(1-\langle\Phi^{-1}|\phi'^*\rangle)]\phi'^*, \tag{88}$$

which can be directly compared to the DNS data of Overholt and Pope.[21] As noted above, a necessary condition for the scalar pdf to be Gaussian is that the right-hand side of this expression be linear in ϕ'^*. In general, this will not be the case and, hence, small-scale inhomogeneities in the scalar dissipation rate will lead to a non-Gaussian scalar pdf.

For the homogeneous, uniform mean-scalar-gradient flow under consideration, if they are initially Gaussian, the $\mathscr{W}$-conditioned components of the scalar-gradient field will also remain Gaussian. However, they need not be uncorrelated. Thus, the standardized random variable Z appearing in Eq. (53) will be the modulus of a correlated Gaussian random vector:

$$Z^2 = \frac{\psi_i\psi_i}{\langle\psi_k\psi_k\rangle}, \tag{89}$$

and a model is required to describe the correlation. In this study, three cases will be compared with DNS data for ϵ^*. All three cases can be modeled by a Fokker–Planck-type model:[19,20]

$$dZ = \omega_\phi^\dagger\left(\frac{N_z-1}{N_z Z} - Z\right)dt + \left(\frac{2}{N_z}\omega_\phi^\dagger\right)^{1/2} dW_z, \tag{90}$$

where $1 \leqslant N_z \leqslant 3$ is the number of uncorrelated components on the right-hand side of Eq. 89. (An equivalent IEM-type model can also be employed that fixes Z constant, i.e., depending only on the initial conditions.) The first case to be considered takes all three components to be uncorrelated ($N_z=3$). The second case assumes only two components are uncorrelated ($N_z=2$). And the third case assumes the scalar field to be locally one-dimensional as seen experimentally in high-Sc flows[51] ($N_z=1$). Given Z, the scalar dissipation can be found from Eq. (53). In Sec. IV, a direct comparison of the scalar dissipation statistics with DNS data will be carried out. Of particular interest is the conditional scalar dissipation:

$$\langle\epsilon_\phi|\phi'^*\rangle = \langle\langle\epsilon_\phi\rangle^* Z^2 | \phi'^*\rangle. \tag{91}$$

Since the ''noise'' term in Eq. (85) would need to be constant, a necessary condition for a Gaussian scalar pdf is that this expression be independent of ϕ'^*. Again, in general, this will not be the case due to small-scale inhomogeneities in the scalar dissipation rate.

D. Conditional scalar flux

In order to complete the Lagrangian pdf description of a scalar field with a uniform mean scalar gradient, models for the conditional scalar flux terms appearing in Eq. (83) are required. These models should be consistent with the analogous $\mathscr{W}$-conditioned terms in the LSR model. In Sec. IV, we will employ the ''standard'' model for the conditional scalar variance source term at a single point in a statistically homogeneous scalar field:

$$\langle u_i|\phi'^*, \mathscr{W}\rangle \frac{\partial\langle\phi\rangle}{\partial x_i} dt = -(S_{\phi^2})^{1/2}\, dW_s, \tag{92}$$

which generates a Gaussian scalar pdf when S_{ϕ^2} is non-zero. It is important to observe that the Wiener process on the

right-hand side of Eq. (92) is delta-correlated, while the velocity field will have a non-zero auto-correlation time proportional to $1/\langle\omega\rangle$. Thus, the model will not generate a realistic Lagrangian time series for ϕ^*. This, however, will not affect the LSR model's predictions since they are independent of ϕ^*. Also note that Eq. (92) would not be required if the velocity were included as a random variable, in which case the scalar flux term is closed[3,12,45] and generates a Gaussian scalar pdf in homogeneous turbulence with a uniform mean scalar gradient.[44]

The model chosen for conditional advection,

$$\left\langle u_i \frac{\partial \phi'}{\partial x_i} \middle| \phi'^*, \mathscr{W} \right\rangle = [\alpha_1 f_1^c(\langle \phi_1'^2 \rangle^* - \langle \phi_1'^2 \rangle) + \cdots + \alpha_{2,n_2} f_{2,n_2}^c(\langle \phi_{2,n_2}'^2 \rangle^* - \langle \phi_{2,n_2}'^2 \rangle)] \frac{\phi'^*}{\langle \phi'^2 \rangle^*}, \tag{93}$$

being linear in ϕ'^*, also admits a $\mathscr{W}$-conditioned Gaussian scalar pdf. However, in general, it will leave the shape of the conditional scalar pdf unchanged, reflecting the fact that only molecular diffusion at small scales (and not inertial-range turbulent mixing) will modify the shape of the scalar pdf of a homogeneous scalar field.[3] Note that, in general, a closure will be required for the conditional advection term, even if the velocity is used as a random variable, in which case the conditioning variables would include $\tilde{u}_i$ and a model would be needed for

$$\left\langle u_i' \frac{\partial \phi'}{\partial x_i} \middle| \tilde{u}_i, \phi'^*, \mathscr{W} \right\rangle. \tag{94}$$

[One can argue that the left-hand side of Eq. (93) need only contain u_i' in place of u_i since the conditional advection with respect to $\tilde{u}_i$ should be null in homogeneous turbulence.[57]] Indeed, although the magnitude of $u_i' dt \sim \eta$ is small compared to $\tilde{u}_i\, dt \sim Re_1^{1/2}\eta$, it is of the same order of magnitude as the size of the fluid particle. Thus, Eq. (93) represents the sole mechanism for inertial-range ''homogenization'' of the scalar field (the right-hand side will be null if the scalar field is homogeneous above the Kolmogorov scale). In general, Eq. (93) will be non-zero only when a ''non-equilibrium'' initial scalar field is employed (e.g., the scalar field is statistically homogeneous at the velocity integral scale, but contains regions with different initial scalar spectral distributions). For this case, the conditional advection term,

$$\left\langle u_i \frac{\partial \phi'}{\partial x_i} \middle| \phi'^* \right\rangle, \tag{95}$$

may be non-linear in ϕ'^*, leading to transient non-Gaussian scalar pdfs as seen in DNS.[22] As shown in Sec. IV, this effect is most pronounced in the absence of a mean scalar gradient [i.e., when Eq. (92) is null].

IV. APPLICATION OF THE LSR MODEL TO HOMOGENEOUS FLOWS

The SR model has been shown[4] to yield satisfactory agreement with available DNS and experimental data for (i) stationary turbulence with a uniform mean scalar gradient,[1] (ii) stationary turbulence with zero mean scalar gradient,[10] (iii) decaying grid turbulence with zero mean scalar gradient,[7] and (iv) decaying grid turbulence with a uniform mean scalar gradient.[8] In particular, the sensitive dependence of the mechanical-to-scalar time-scale ratio on the initial scalar spectrum is successfully captured by the SR model due to its explicit representation of scalar spectral transport by a local cascade between finite-sized wavenumber bands. Since the LSR model contains a nearly identical spectral description, its predictions for the dynamical behavior of the *mean* scalar dissipation rate in the above flows mimics the SR model. Thus, the focus of the present section is on the ability of the LSR model to predict pdf and higher-order statistics for the scalar and the scalar dissipation in stationary, isotropic turbulence. Results for two cases will be considered: (A) stationary and (B) transient statistics for a passive scalar with and without a uniform mean scalar gradient. For case A, model predictions will be compared with the extensive DNS results of Overholt and Pope[21] for the joint statistics of the scalar, scalar gradient, and the turbulent frequency at two Reynolds numbers. For case B, model predictions show a sensitive dependence on the initial scalar spectrum, and a transient non-Gaussian scalar pdf can result due to large-scale inhomogeneity of the scalar field. For this case, a quali-

TABLE I. Stationary moments of the pdf of the turbulent frequency ($X=\omega/\langle\omega\rangle$) found from Eq. (58) with $C_\omega=0.35$, $C_\chi=1$, $h=0$, $S_\omega=0$, and $\langle\omega\rangle=1$. DNS values are shown in parentheses.

$R_\lambda(\gamma_{\omega 1})$	28 (0.778)	84 (0.500)
Variance, σ_ω^2	0.702 ± 0.023 (0.783 ± 0.026)	1.24 ± 0.01 (1.25 ± 0.09)
Skewness	2.23 ± 0.02 (2.32 ± 0.03)	3.85 ± 0.09 (3.62 ± 0.12)
Kurtosis	11.9 ± 0.4 (11.8 ± 0.4)	34.8 ± 3.7 (28.4 ± 2.6)
Superskewness	672 ± 183 (499 ± 59)	11400 ± 8700 (4900 ± 1440)

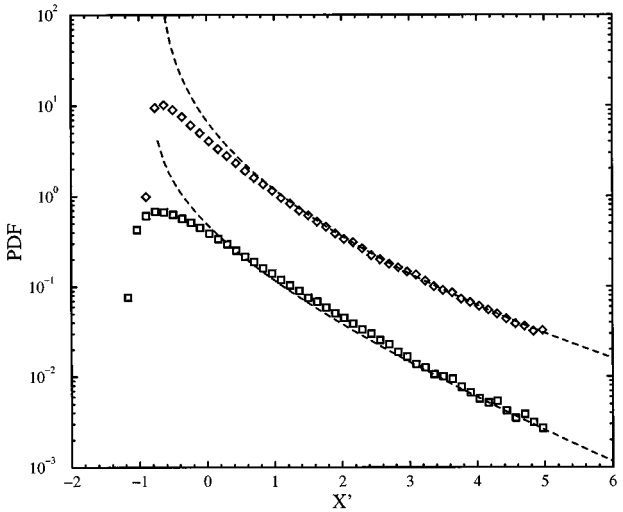

FIG. 1. Stationary pdf of the turbulent frequency $[X'=(\omega^*-\langle\omega\rangle)/\sigma_\omega]$ found with $C_\chi=1$, $C_\omega=0.35$, $h=0$, $S_\omega=0$, and $\langle\omega\rangle=1$. □: $R_\lambda=28$ ($\gamma_{\omega 1}=0.778$). ◇: $R_\lambda=84$ ($\gamma_{\omega 1}=0.500$), shifted up one decade. The dashed curves correspond to the stretched-exponential pdf fitted using DNS data.[21]

TABLE II. Stationary moments of the pdf of the natural logarithm of the turbulent frequency $[\ln(X)]$ found with the parameters in Table I.

R_λ	28	84
Variance, $\sigma^2_{\ln(X)}$	0.730 ± 0.001 (0.728 ± 0.003)	1.030 ± 0.002
Skewness	-0.496 ± 0.004 (-0.335 ± 0.005)	-0.354 ± 0.003
Kurtosis	3.58 ± 0.01 (3.31 ± 0.01)	3.39 ± 0.01
Superskewness	28.5 ± 0.5 (22.5 ± 0.3)	23.2 ± 0.3

TABLE III. Stationary moments of the scalar pdf with $f_D=1$. First three rows: $S_{\phi^2}=1$. Last two rows: $S_{\phi^2}=0$. DNS values are shown in parentheses.

R_λ, Sc, N_z	28, 1, 1	84, 1, 1	84, 1, 3	84, 200, 1
Variance, σ^2_ϕ	1.04	1.03	1.03	1.12
Kurtosis	3.03 (2.90 ± 0.03)	3.05 (2.86 ± 0.10)	3.01	3.08
Superskewness	15.4 (13.6 ± 0.4)	15.7 (13.1 ± 1.2)	15.2	16.2
Kurtosis	3.08	3.09	3.02	3.13
Superskewness	16.3	16.4	15.0	17.0

tative comparison of the transient statistics predicted by the LSR model with the DNS data of Jaberi *et al.*[22] is presented.

A. Stationary scalar statistics in isotropic turbulence

The first case to be considered is the asymptotic behavior for scalar mixing in forced, isotropic turbulence. At the statistically stationary (SS) state, $\langle r_\phi\rangle$ is constant and, in the presence of a uniform mean scalar gradient, $\langle\epsilon_\phi\rangle=S_{\phi^2}$. Thus, when $0<S_{\phi^2}$, the stationary LSR model simplifies significantly since $\langle\phi_1'^2\rangle=\langle\phi_1'^2\rangle^*$, $\langle\phi_{2,j}'^2\rangle=\langle\phi_{2,j}'^2\rangle^*$, and the right-hand sides of Eqs. (63)–(65) are null. Similar simplifications result in the absence of a mean scalar gradient if the model equations are rewritten in terms of fraction of scalar energy in a wavenumber band, i.e., $\langle\varsigma_{i,j}\rangle^\dagger$. At the SS state, the mean spectral fractions become constant, and fluctuations in $\langle\epsilon_\phi\rangle^*$ are generated by $\sigma(t)$ in Eq. (70); hence, as noted earlier, the statistics of ω^* play a crucial role in determining the scalar statistics.

1. Turbulent frequency statistics

In Table I, results for the dimensionless turbulent frequency,

$$X=\frac{\omega^*}{\langle\omega\rangle},$$

found from Monte-Carlo simulations of Eq. (58) (hereinafter all simulations employ $N=10^6$ notional particles unless noted otherwise) are compared with the DNS data for two values of R_λ. The model constant $C_\omega=0.35$ in Eq. (62) was fitted by forcing the model variance (σ^2_ω) to agree with the DNS variance at $R_\lambda=84$. In general, it can be seen that within the bounds of statistical error the model satisfactorily reproduces the DNS results, including the dependence on R_λ. (Recall, however, that $\gamma_{\omega 1}$ supplies the R_λ dependence, and it is an input to the model.) Stationary pdfs for the standardized turbulent frequency,

$$X'=\frac{\omega^*-\langle\omega\rangle}{\sigma_\omega},$$

are shown in Fig. 1. For comparison, the stretched-exponential pdf fitted to DNS data by Overholt and Pope[21] is shown by a dashed line. As expected from the choice of the model parameters, the upper tails of the simulated pdfs are in excellent agreement with the DNS stretched-exponential forms. [This would not be the case if, for instance, Eq. (57) were employed to model ω^*.] Similar results for $\ln(X)$ are presented in Table II and Fig. 2 where again satisfactory agreement with the DNS data is observed. In order to highlight the non-log-normality of X, a Gaussian pdf has been included in Fig. 2. Note that unlike Eq. (57), Eq. (58) predicts significant negative skewness for $\ln(X)$. In conclusion, it is found that Eq. (58) yields a satisfactory description of the one-point, one-time turbulent frequency statistics ob-

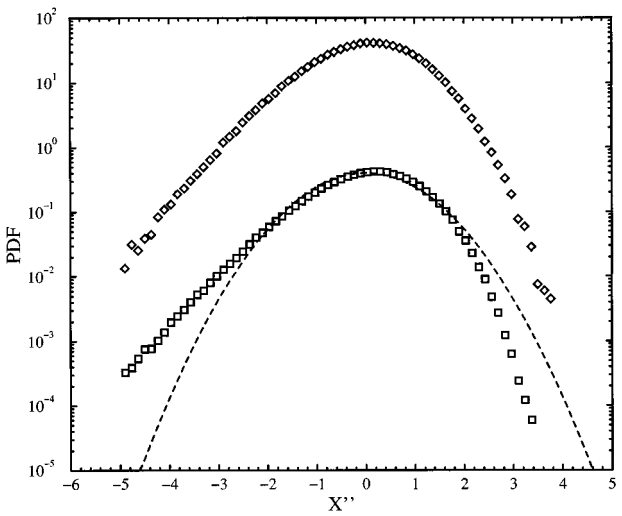

FIG. 2. Stationary pdf of the natural logarithm of the turbulent frequency $[X''=(\ln(X)-\langle\ln(X)\rangle)/\sigma_{\ln(X)}]$ found with parameters in Fig. 1. □: $R_\lambda=28$; ◇: $R_\lambda=84$, shifted up two decades; dashed curve: Gaussian pdf.

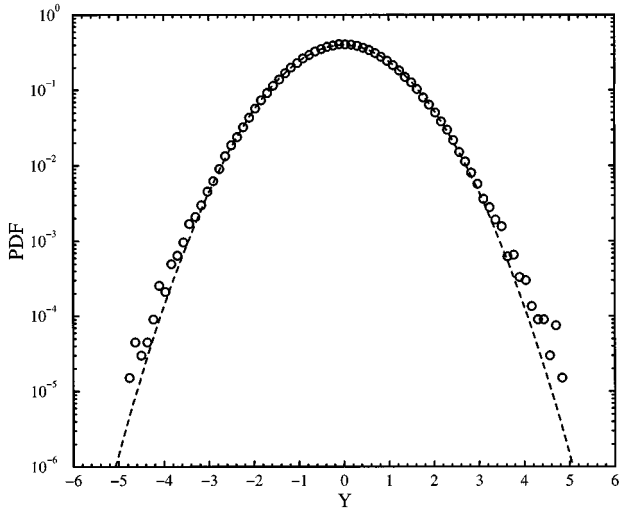

FIG. 3. Stationary scalar pdf $(Y=\phi'^*/\sigma_\phi)$ found with $S_{\phi^2}=0$, $R_\lambda=84$, $Sc=200$, $N_z=1$, and $f_D=1$. All other parameters are the same as in Fig. 1. Dashed curve: Gaussian pdf.

TABLE IV. Stationary moments of the pdf of the scalar dissipation ($X_\phi = \epsilon_\phi / \langle \epsilon_\phi \rangle$) with a uniform mean scalar gradient ($S_{\phi^2} = 1$) and $f_D = 1$. DNS values are shown in parentheses. N_z is the number of uncorrelated scalar-gradient components in the model for Z.

R_λ, Sc, N_z	28, 1, 1	84, 1, 1	84, 1, 2	84, 1, 3	84, 200, 1
Variance, $\sigma^2_{\epsilon_\phi}$	2.14 (2.97±0.31)	2.72 (5.68±2.17)	1.13	0.717	3.85
Skewness	3.14 (4.28±0.07)	4.82 (6.89±0.61)	2.42	1.80	5.65
Kurtosis	18.9 (31.5±1.2)	54.5 (84.2±16.8)	13.3	8.12	65.4
Superskewness	1485 (3200±370)	31400 (28600±12200)	846	251	35600

tained from DNS. The effect of the autocorrelation time (i.e., C_χ) will be explored below in relation to joint scalar dissipation, turbulent frequency statistics.

Given a model for ω^* (and hence $\mathscr{W}$) the LSR model can be employed to predict joint scalar, scalar dissipation, turbulent frequency statistics as a function of R_λ, Sc, and N_z. As noted in Sec. III, only the case where V and Z are independent, Gaussian random fields will be considered in this work. This implies that either Eq. (84) or Eq. (85) (and the corresponding expressions for Z) can be used to close the molecular mixing term. (Simulations have been carried out with both models and statistically identical results were found.) Note that the parameter N_z enters the LSR model both through the initialization of Z and in the parameters C_s and C_d. For the range of Reynolds numbers considered ($R_\lambda \leqslant 84$), a maximum of $n_2 = 3$ substages are required to describe the inertial subrange of the scalar spectrum.[4] Likewise, two Schmidt numbers ($Sc = 1$ and 200) have been investigated and correspond, respectively, to $n_3 = 0$ and $n_3 = 1$. Finally, in order to treat the zero-mean-gradient case, the LSR model equations were rewritten in terms of the ''local'' spectral fractions (i.e., $\langle \varsigma_{i,j} \rangle^\dagger = \langle \phi'^2_{i,j} \rangle^* / \langle \phi'^2 \rangle^*$) and the ''local'' scalar dissipation rate ($\omega^\dagger_\phi$). Thus, each notional particle in a Monte-Carlo simulation carries the following random variables: ω^*, $\langle \varsigma_1 \rangle^\dagger$, $\langle \varsigma_{2,1} \rangle^\dagger$, $\langle \varsigma_{2,2} \rangle^\dagger$, $\langle \varsigma_{2,3} \rangle^\dagger$, $\langle \varsigma_{3,1} \rangle^\dagger$, Φ, and $\omega^\dagger_\phi$.

2. Scalar statistics

As noted in Sec. III, a non-Gaussian scalar pdf can result from the LSR model due to fluctuations in the ''local'' scalar-variance ratio (i.e., Φ). This ''small-scale intermittency'' route to non-Gaussian behavior is evident in Table III and in Fig. 3 where the tails of the scalar pdf decay more slowly than the quadratic dependence seen with a Gaussian pdf. Nearly identical tails are obtained from DNS.[59] From Table III, it can be observed that, as expected, non-Gaussian behavior is greatest in the absence of a mean scalar gradient. (DNS of the zero-mean-gradient case is difficult due to the sensitive dependence on the initial scalar spectrum and to the rapid decay of scalar fluctuations.) The predicted dependence on Reynolds number is more subtle (increasing R_λ increases the variance of ω^*, but decreases the fraction of the scalar spectrum subject to turbulent fluctuations as discussed below); however, a slight increase (linked to an increase in the variance of Φ) is observed at $R_\lambda = 84$. On the other hand, it is clearly seen that increasing the Schmidt number leads to a significant increase in non-Gaussian behavior (no DNS data is available for large Sc), while increasing N_z leads to a decrease. Physically, one can contribute the N_z dependence to a decrease in the scalar dissipation variance (discussed below). The Sc dependence can be understood in a similar manner: increasing Sc leads to a larger fraction of the scalar spectrum in the viscous-convective subrange (i.e., stage 3) where it is directly subject to turbulent-frequency fluctuations, thereby increasing the scalar dissipation variance.

3. Scalar dissipation statistics

The LSR model predictions for the scalar dissipation are presented in Tables IV and V. All of the simulation results for the scalar dissipation show a very weak (negligible) dependence on S_{ϕ^2}. Looking first at results for the normalized scalar dissipation,

$$X_\phi = \frac{\epsilon^*_\phi}{\langle \epsilon_\phi \rangle},$$

it can be seen that the LSR model captures the large values of the skewness, kurtosis, and superskewness (and their R_λ dependence) seen in the DNS results. (As reflected in the error bounds, due to the large number of extreme values present, it is difficult to determine if these moments are sample-size independent. Compare the results with Table IX where the sample size is 10^5.) Note, however, that the model generally underpredicts the variance and its scaling with R_λ. This trend persists for other values of C_χ (Table IX), but improves with increasing Sc. This observation suggests that coherent turbulent-frequency fluctuations (which were assumed to exist only for wavenumbers greater than κ_U) may

TABLE V. Stationary moments of the pdf of the natural logarithm of the scalar dissipation [$\ln(X_\phi)$] with $S_{\phi^2} = 0$ and $f_D = 1$.

R_λ, Sc, N_z	28, 1, 1	84, 1, 1	84, 1, 2	84, 1, 3	84, 200, 1
Variance, $\sigma^2_{\ln(X_\phi)}$	5.00 (1.98±0.02)	5.13	1.75	0.987	5.65
Skewness	-1.50 (−0.204±0.008)	-1.44	-1.06	-0.881	-1.27
Kurtosis	6.90 (3.09±0.01)	6.66	5.04	4.55	6.08
Superskewness	157 (18.8±0.3)	146	68.5	58.5	121

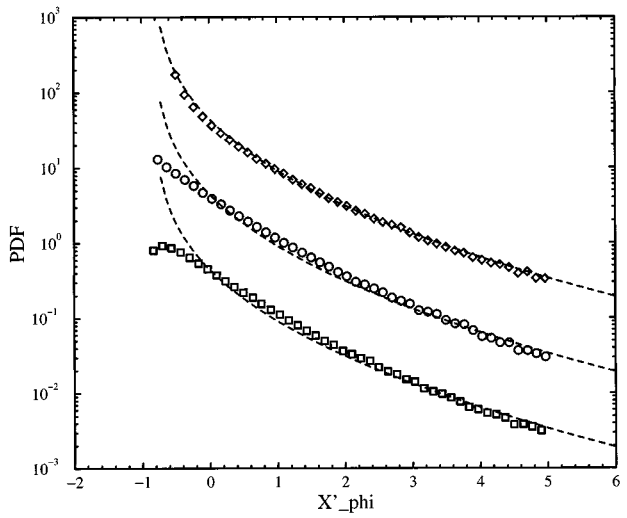

FIG. 4. Stationary pdf of the scalar dissipation $[X'_\phi=(\epsilon^*_\phi-\langle\epsilon_\phi\rangle)/\sigma_{\epsilon_\phi}]$ found with $R_\lambda=84$, $Sc=1$, $S_{\phi^2}=1$, and $f_D=1$. All other parameters are the same as in Fig. 1. □: $N_z=3$; ○: $N_z=2$, shifted up one decade; ◇: $N_z=1$, shifted up two decades. The dashed curves correspond to the stretched-exponential pdf fit using DNS data.[21]

extend back into stage 2, and that the LSR model may be further improved by including a dependence on $\sigma(t)$ at the end of this stage. [Note that for $Sc=1$, the first term of the right-hand side of Eq. (70) contains α_{2,n_2} in place of $\alpha_3\sigma(t)$. This has the result of artificially reducing fluctuations in $\langle\epsilon_\phi\rangle^*$ (cf. Fig. 7) as compared to cases where $1<Sc$.] This modification can be implemented by introducing an additional wavenumber band to represent the beginning of the velocity-dissipation range[34] (i.e., the end of the inertial range): $\kappa_I=C_I^{3/2}\kappa_K$ where $C_I=C_U/2$, an additional substage (n_2+1) in stage 2 with a convective transport rate,

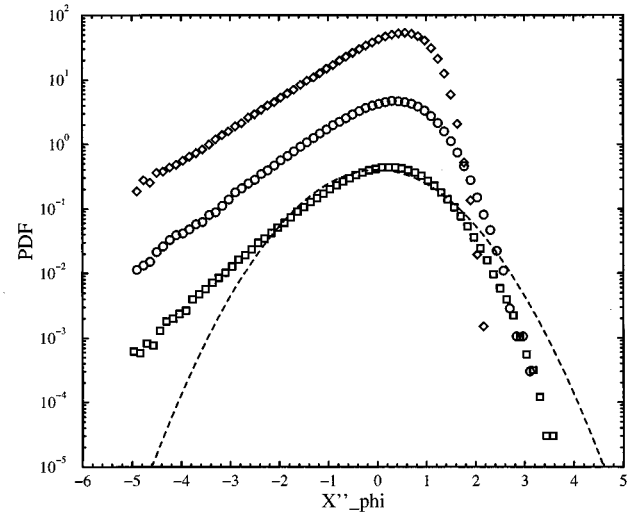

FIG. 5. Stationary pdf of the natural logarithm of the scalar dissipation $[X''_\phi=(\ln(X_\phi)-\langle\ln(X_\phi)\rangle)/\sigma_{\ln(X_\phi)}]$ found with $R_\lambda=84$ and $S_{\phi^2}=0$. All other parameters are the same as in Fig. 4. □: $N_z=3$; ○: $N_z=2$, shifted up one decade; ◇: $N_z=1$, shifted up two decades; dashed curve: Gaussian pdf.

TABLE VI. Stationary mechanical-to-scalar time-scale ratio, correlation coefficients, and the standard deviation of Φ with $f_D=1$. DNS values are shown in parentheses. First four rows: $S_{\phi^2}=1$. Last four rows: $S_{\phi^2}=0$.

R_λ, Sc, N_z	28, 1, 1	84, 1, 1	84, 1, 2	84, 1, 3	84, 200, 1
$\langle r\rangle$	1.92 (1.82)	1.95 (2.22)	1.94	1.94	1.79
$\rho(\phi^2,\epsilon_\phi)$	-0.006 (-0.022)	-0.008 (-0.021)	-0.003	-0.001	-0.012
$\rho(\epsilon,\epsilon_\phi)$	0.116 (0.235)	0.217 (0.165)	0.176	0.146	0.273
σ_Φ	0.092	0.120	0.075	0.054	0.159
$\langle r\rangle$	2.00	2.00	2.00	2.00	2.00
$\rho(\phi^2,\epsilon_\phi)$	0.002	0.001	0.001	0.000	0.002
$\rho(\epsilon,\epsilon_\phi)$	0.116	0.209	0.180	0.154	0.246
σ_Φ	0.164	0.173	0.117	0.088	0.205

$$\alpha_{2,n_2+1}\sigma(t)=\tfrac{2}{3}C_U Re_1\sigma(t),$$

and by replacing C_U with C_I in, for example, Eqs. (14) and (33). [Note that, due to the separation-of-scales condition, $1<C_I Re_1$ $(42<R_\lambda)$, care must be taken when applying the

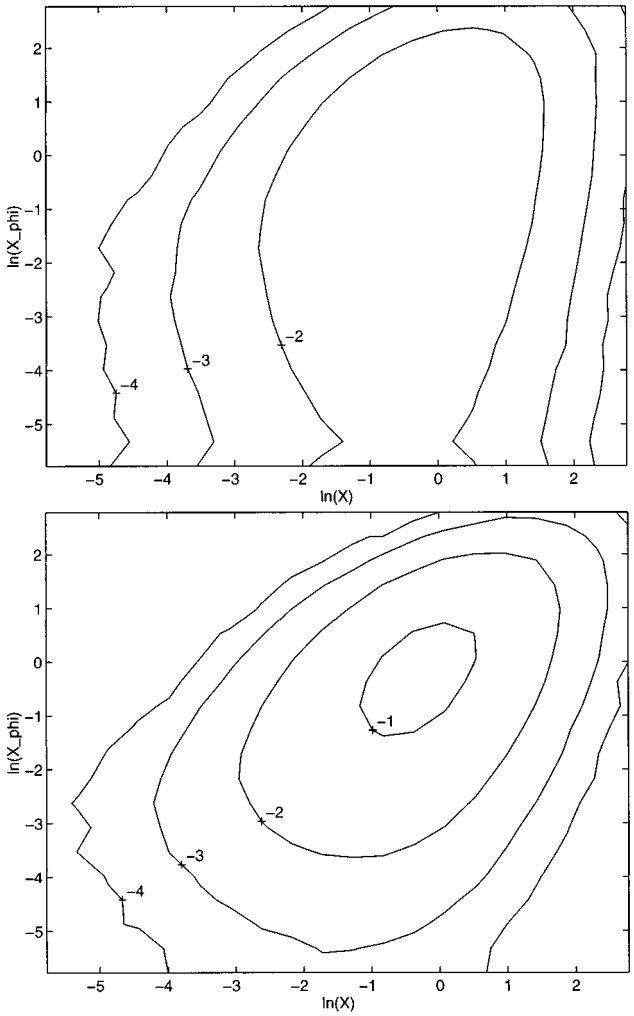

FIG. 6. Stationary joint pdf of the natural logarithm of the turbulent frequency $[\ln(X)]$ and of the scalar dissipation $[\ln(X_\phi)]$. All other parameters are the same as in Fig. 4. Top: $N_z=1$; bottom: $N_z=3$. Contour levels: $-1{:}10^{-1}$, $-2{:}10^{-2}$, $-3{:}10^{-3}$, $-4{:}10^{-4}$.

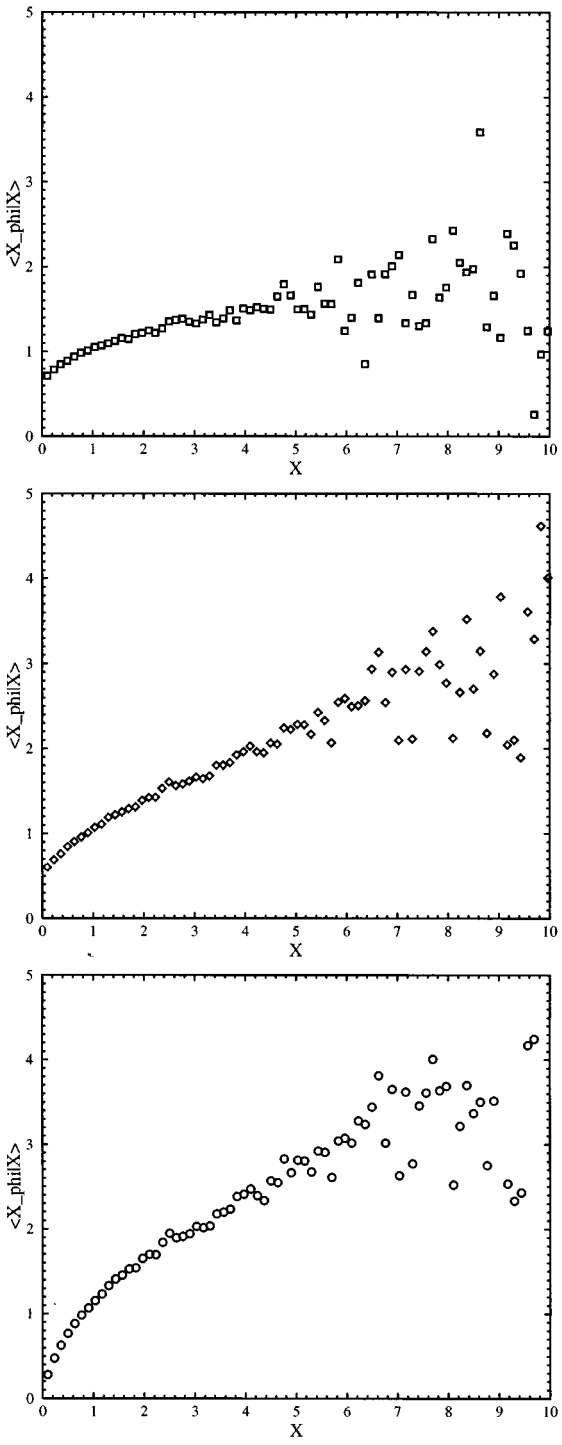

FIG. 7. Stationary conditional expectation of the scalar dissipation (X_ϕ) given the turbulent frequency (X) with $N_z=1$. □: $R_\lambda=28$, $Sc=1$; ◇: $R_\lambda=84$, $Sc=1$; ○: $R_\lambda=84$, $Sc=200$. All other parameters are the same as in Fig. 4.

modified model to low Reynolds number flows where the integral and dissipation scales are not clearly separated.]

The generally good agreement with the DNS results is also reflected in the pdf of the standardized scalar dissipation (Fig. 4):

$$X'_\phi=\frac{\epsilon^*_\phi-\langle\epsilon_\phi\rangle}{\sigma_{\epsilon_\phi}},$$

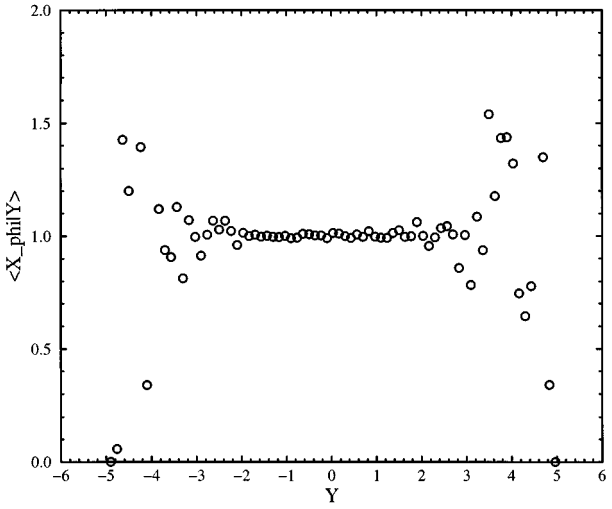

FIG. 8. Stationary conditional expectation of the scalar dissipation (X_ϕ) given the scalar (Y). All other parameters are the same as in Fig. 3.

which has the characteristic stretched-exponential form seen in earlier studies.[21,50,60] In Fig. 4, the dashed curves are again the stretched-exponential forms fitted to the DNS data by Overholt and Pope.[21] Note that the behavior of the pdf for large values of X'_ϕ is dominated by the behavior of $\langle\epsilon_\phi\rangle^*$. Thus, the stretched-exponential tails seen in Fig. 4 are a direct result of having stretched-exponential tails for the pdf of ω^*. (This result has been confirmed by simulations employing alternative models for ω^*.) On the other hand, the behavior for small values of X'_ϕ is dominated by the behavior of Z^2. For small Z^2, its pdf scales like $f(x)\sim x^{N_z/2-1}$, and this scaling is clearly seen in Fig. 4. Similar conclusions can be drawn from the results for $\ln(X_\phi)$ presented in Table V and Fig. 5 where it can be observed that the model moderately overpredicts the magnitude of the moments. This result can be traced to an underprediction of the fall-off rate of the left-hand tail of the pdf (Fig. 5) as compared to the DNS results.[17]

4. Joint statistics

Additional stationary statistics are presented in Table VI. Note that the value of the mechanical-to-scalar time-scale ratio is controlled, primarily, by the choice of the integral-scale time-scale t_1 [Eq. (32)] which will be affected, for example, by the forcing scheme employed in the DNS.[59] In the LSR model, t_1 is chosen to be $1/\langle\omega\rangle$, and thus $\langle r\rangle$ is nearly independent of R_λ. The model's agreement with DNS could thus be improved by incorporating the R_λ-dependence seen in the DNS results. Also note that the turbulent-dissipation, scalar-dissipation correlation coefficient, $\rho(\epsilon,\epsilon_\phi)$, predicted by the model is near the (positive) DNS value. (The model value is dependent on C_χ as seen in Table IX, but is always positive.) This results from the relatively strong correlation between ω^* and $\langle\epsilon_\phi\rangle^*$ that is clearly evident in Figs. 6 and 7, and in similar figures from DNS[21] that show precisely the same trend. Indeed, in Fig. 7, the scalar dissipation conditioned on the turbulent frequency,

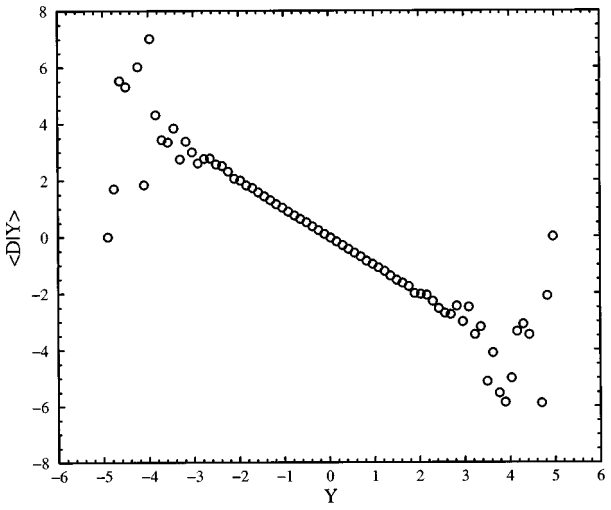

FIG. 9. Stationary conditional expectation of the scalar Laplacian $[D=(\Gamma\nabla^2\phi')/(\langle r_\phi\rangle\sigma_\phi)]$ given the scalar (Y). All other parameters are the same as in Fig. 3.

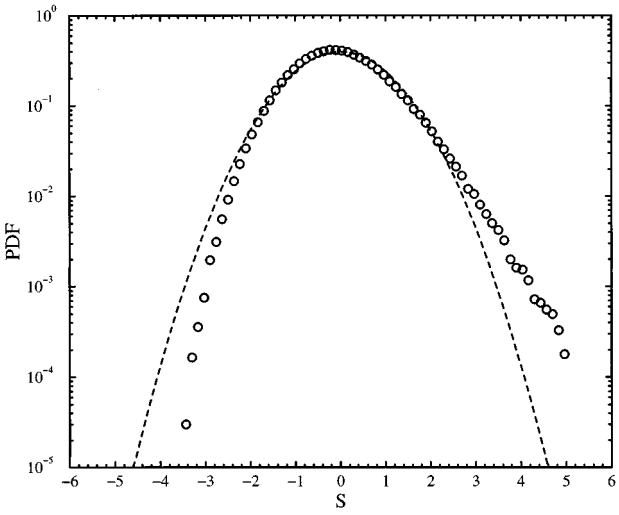

FIG. 10. Stationary pdf of the scalar–variance ratio $(S=(\Phi-\langle\Phi\rangle)/\sigma_\Phi)$. Dashed curve: Gaussian pdf. All parameters are the same as in Fig. 3.

$$\langle X_\phi|X=x\rangle=\left\langle\frac{\epsilon_\phi}{\langle\epsilon_\phi\rangle}\middle|\frac{\omega^*}{\langle\omega\rangle}=x\right\rangle,$$

shows the same behavior with respect to x as found by DNS, suggesting that Eq. (70) captures the essential physics of the coupling between small-scale turbulent-frequency fluctuations and scalar dissipation. As discussed in greater detail below, the fact that the autocorrelation time of ω^* is finite and of the same order of magnitude as that of $\langle\epsilon_\phi\rangle^*$ in the LSR model is also significant in determining the form of the conditional scalar dissipation.

The model predicts, in good agreement with DNS, that the scalar, scalar-dissipation correlation coefficient, $\rho(\phi^2,\epsilon_\phi)$, is nearly zero. The lack of significant correlation between the scalar and scalar dissipation is also observed in Fig. 8 for the conditional statistic:

$$\langle X_\phi|Y=x\rangle=\left\langle\frac{\epsilon_\phi}{\langle\epsilon_\phi\rangle}\middle|\frac{\phi'^*}{\sigma_\phi}=x\right\rangle,$$

and in Fig. 9 for the conditional scalar Laplacian:

$$\langle D|Y=x\rangle=\left\langle\frac{\Gamma\nabla^2\phi'}{\langle r_\phi\rangle\sigma_\phi}\middle|\frac{\phi'^*}{\sigma_\phi}=x\right\rangle.$$

TABLE VII. Stationary moments of the pdf of the scalar–variance ratio (Φ) with $f_D=1$. First three rows: $S_{\phi^2}=1$. Last three rows: $S_{\phi^2}=0$.

R_λ, Sc, N_z	28, 1, 1	84, 1,1	84, 1, 3	84, 200, 1
Skewness	-0.09	-0.53	-0.53	0.00
Kurtosis	2.86	3.35	3.61	3.10
Superskewness	13.1	22.0	30.0	16.0
Skewness	0.52	0.05	-0.14	0.40
Kurtosis	3.48	3.04	3.14	3.50
Superskewness	25.9	15.5	17.3	26.5

Note that a sufficient condition for a Gaussian scalar pdf is that the curves in both figures be linear in x as appears to be the case for $-3\leqslant Y\leqslant 3$ (cf. Fig. 3). Nearly identical behavior is found from DNS.[21]

5. Scalar-variance ratio statistics

Stationary moments for the scalar-variance ratio are presented in Tables VI and VII. As noted earlier, Φ plays a key role in determining the extent of non-Gaussian behavior in the scalar pdf. As is evident from Table VI, the magnitude of the fluctuations in Φ, as measured by the standard deviation σ_Φ, is strongly correlated with the extent of non-Gaussianity in Table III. The higher-order moments in Table VII indicate that the shape of the pdf is strongly dependent on the simulation parameters. For example, the pdf of

$$S=\frac{\Phi-\langle\Phi\rangle}{\sigma_\Phi},$$

for $Sc=200$ shown in Fig. 10 is slightly shewed towards positive values. As expected from the model formulation, the presence of a mean scalar gradient greatly reduces σ_Φ. The effect of reducing the diffusive-mixing parameter, f_D, is shown in Table VIII where it can be seen that smaller values of f_D lead to larger fluctuations in Φ and eventually to numerical instability. In theory, DNS data could be employed to estimate f_D from the diffusive-mixing model:

TABLE VIII. Effect of diffusive-mixing parameter (f_D) on selected stationary scalar statistics with $R_\lambda=84$, $Sc=1$, $N_z=1$, and $S_{\phi^2}=0$. When $f_D\leqslant 0.4$, the simulation becomes statistically unstable before attaining a statistically stationary state.

f_D	1.0	0.8	0.6	0.4
σ_Φ	0.171	0.218	0.234	0.366
Kurtosis	3.09	3.15	3.17	3.13
Superskewness	16.4	16.4	17.7	17.0

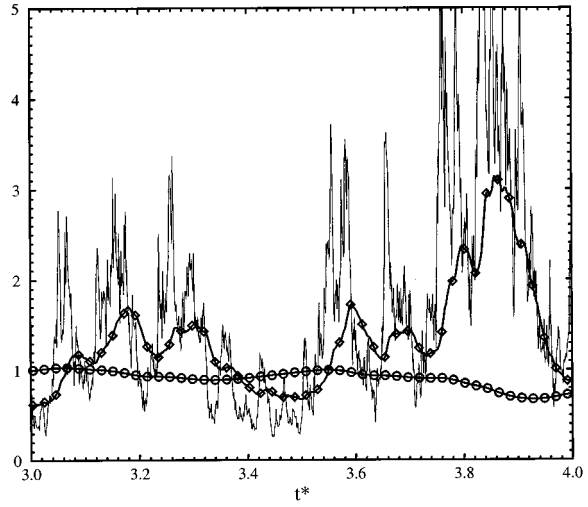

FIG. 11. Example Lagrangian time series following a notional particle found with $R_\lambda = 84$ and $Sc = 1$. The dimensionless time is defined by $t^* = \langle\omega\rangle t$. All other parameters are the same as in Fig. 4. Solid line: ω^*; $\diamond$: $\omega_\phi^\dagger$; $\bigcirc$: Φ.

$$f_D(\langle\phi'^2\rangle - \langle\phi'^2|\mathscr{W}\rangle) = \frac{\langle\Gamma\nabla^2\phi'^2|\mathscr{W}\rangle}{2\langle r_\phi\rangle},$$

but this would require Lagrangian conditional statistics that are difficult to obtain with sufficient accuracy from DNS with $Sc \approx 1$. Note, however, that the effective sample size of the scalar field in a Kolmogorov-scale fluid particle can be increased by using larger values of Sc for which DNS is unfeasible. For this case, it may be possible to extract conditional statistics from high-Sc experimental data[51] where, for example, the conditional variance $\langle\phi'^2|\mathscr{W}\rangle$ would correspond to the variance in a 3-D, Kolmogorov-scale measurement window at a fixed time, and multiple samples could be obtained by extracting data over many instants in time.

6. Temporal statistics

The one-point, one-time statistics presented thus far provide no information about the temporal behavior of the stochastic models. This information can be extracted from Lagrangian time series such as those presented in Fig. 11 where the dimensionless time is defined by $t^* = \langle\omega\rangle t$. (No DNS Lagrangian statistics for the scalar quantities have been reported in the literature. However, it should possible[61] and of considerable interest to compute them for comparison with model predictions.) Qualitatively, it is clear that the time series for the scalar quantities ($\omega_\phi^\dagger$ and Φ) are smoother than that of the turbulent frequency. Moreover, it can also be observed that peaks in the scalar quantities occur with a short time delay after peaks in the turbulent frequency, and that the time series for Φ is considerably smoother than the other two. These observations can be made quantitative by computing the Lagrangian stationary auto- and cross-correlation functions defined for arbitrary second-order stationary, zero-mean, Lagrangian time series $T_1(t)$ and $T_2(t)$ by

$$\rho_i(\tau) = \frac{\langle T_i(t)T_i(t+\tau)\rangle}{\langle T_i^2(t)\rangle}$$

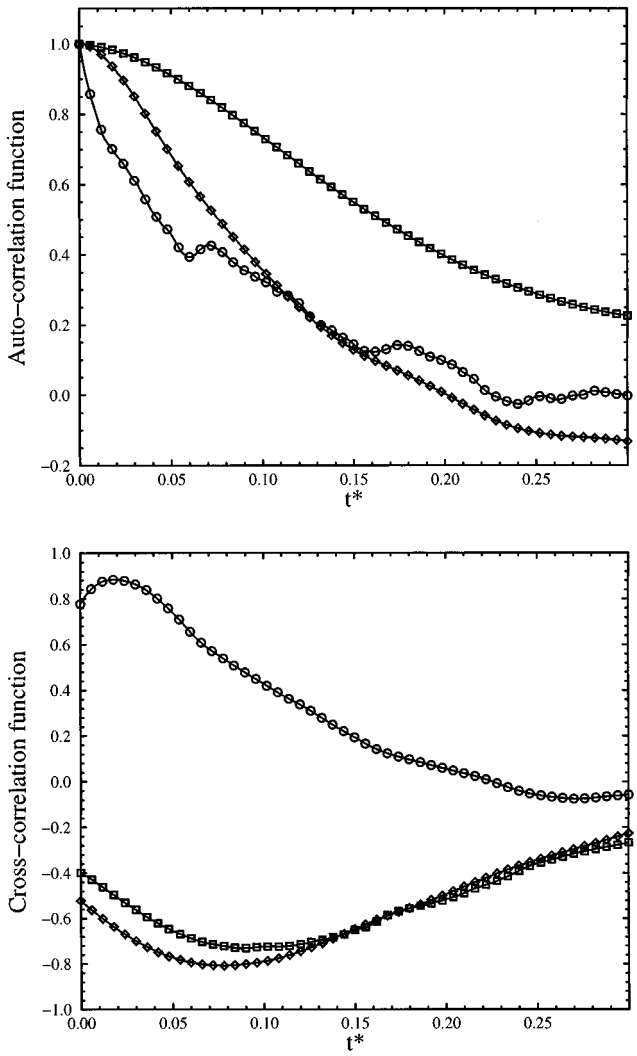

FIG. 12. Lagrangian auto- and cross-correlation functions with $C_\chi = 1$ and all other parameters are as in Fig. 4. Top—$\bigcirc$: ω^*; $\diamond$: $\omega_\phi^\dagger$; $\square$: Φ. Bottom—$\bigcirc$: ω^* and $\omega_\phi^\dagger$; $\diamond$: $\omega_\phi^\dagger$ and Φ; $\square$: ω^* and Φ.

and

$$\rho_{1,2}(\tau) = \frac{\langle T_1(t)T_2(t+\tau)\rangle}{\langle T_1^2(t)\rangle^{1/2}\langle T_2^2(t)\rangle^{1/2}},$$

respectively. (Note that stationarity implies that the right-hand sides are independent of t.) Lagrangian auto- and cross-correlation functions for the LSR model appear in Fig. 12. From the behavior of its auto-correlation function near $t^* = 0$, it can be seen that ω^* becomes uncorrelated exponentially fast [as would be expected for a random process driven by white-noise, Eq. (57)] with a dimensionless auto-correlation time of approximately 0.06 ($\approx 2.8 t_K$ where $t_K = 1/Re_1 = 0.031$ is the dimensionless Kolmogorov time scale). On the other hand, the auto-correlation functions for $\omega_\phi^\dagger$ and Φ both have zero slope at $t^* = 0$, reflecting the fact that their time series are differentiable (or twice differentiable in the case of Φ) and, hence, relatively smooth functions of time. Also note that their auto-correlation times are approximately the same as that of ω^*. The existence of a time delay is confirmed by the cross-correlation functions.

For example, $\omega^*(t^*)$ is most strongly (positive) correlated with $\omega_\phi^\dagger(t^*+0.6t_K)$ and (negative) with $\Phi(t^*+3.2t_K)$, while $\omega_\phi^\dagger(t^*)$ is most strongly (negative) correlated with $\Phi(t^*+2.4t_K)$. Finally, as discussed below, it is important to keep in mind that these results are strongly dependent on the choice of $C_\chi=1$ in the model for ω^*. In particular, if $C_\chi\sim 1/Re_1$ then the auto-correlation times will no longer scale like t_K (Fig. 14).

7. Effect of the auto-correlation time

In the Lagrangian pdf model for ω^*, C_χ controls the auto-correlation time and, since it describes processes near the Kolmogorov scale, the latter is assumed to scale like $1/Re_1$. Nevertheless, available DNS statistics[61] suggest that the Lagrangian auto-correlation time may be independent of Re_1, in which case $C_\chi\sim 1/Re_1$. The effect of C_χ on the predictions of the LRM model has thus been investigated, and the results are presented in Table IX and Figs. 13–15. As noted earlier, a stretched-exponential pdf for the scalar dissipation is predicted for all three values of C_χ (i.e., if the pdf of X is stretched exponential, then so is that of X_ϕ). Nevertheless, C_χ has a strong effect on the correlation coefficient $\rho(\epsilon,\epsilon_\phi)$, and on the magnitude of the moments of the scalar dissipation pdf. Experimentation has revealed that all of these statistics have their maximum values (and are closest to DNS) when $C_\chi\approx 1$. On the other hand, the largest value of σ_Φ occurs with the smallest value of C_χ. The conditional scalar dissipation, presented in Fig. 13, also shows a strong dependence on C_χ. (Qualitatively, the conditional scalar dissipation found with $C_\chi=1/Re_1$ agrees most closely with the DNS results.[21]) For $C_\chi=1/Re_1$, $\langle X_\phi|X=x\rangle$ falls off more quickly with increasing x than is seen with $C_\chi=1$, indicating that large values of the scalar dissipation are less correlated with large values of the turbulent frequency when the auto-correlation time is increased. This behavior can be understood by observing that in the LSR model $X_\phi\sim\omega_\phi^\dagger\Phi$ so that the effect of changing the autocorrelation time will depend on its influence on both $\omega_\phi^\dagger$ and Φ. Scatter plots of these two variables versus ω^* reveal that as C_χ decreases, Φ is more strongly affected, and that for large ω^* the value of Φ becomes significantly smaller as C_χ decreases, thereby decreasing X_ϕ. In the limit $C_\chi\to 0$, the LSR variables will be in a quasi-equilibrium state where all time derivatives are approximately zero. Letting $S=S_{\phi^2}/\langle\phi'^2\rangle$, the model equation for Φ in this limit then yields ($f_D=1$)

$$\Phi=\frac{S+\langle r_\phi\rangle}{S+\omega_\phi^\dagger}.$$

Noting that if $0<S$, then $\langle r_\phi\rangle=S$; the limiting behavior for X_ϕ is thus found to be

$$X_\phi=1,\quad \text{if } S=0$$

or

$$X_\phi=C\frac{\omega_\phi^\dagger}{1+\omega_\phi^\dagger},\quad \text{otherwise,}$$

where $C=1+\langle 1/\omega_\phi^\dagger\rangle$. Note that the second relation above agrees well with the case $C_\chi=1/Re_1$ in Fig. 13, and that the model predicts that ϵ_ϕ^* and ω^* will be nearly uncorrelated in the absence of a mean scalar gradient if $C_\chi\sim 1/Re_1$. The latter has been confirmed from simulations and is in sharp contrast to the case $C_\chi=1$ where the conditional scalar dissipation is nearly the same in the absence of or with a mean scalar gradient. Conversely, when $1\ll C_\chi$ both $\omega_\phi^\dagger$ and Φ

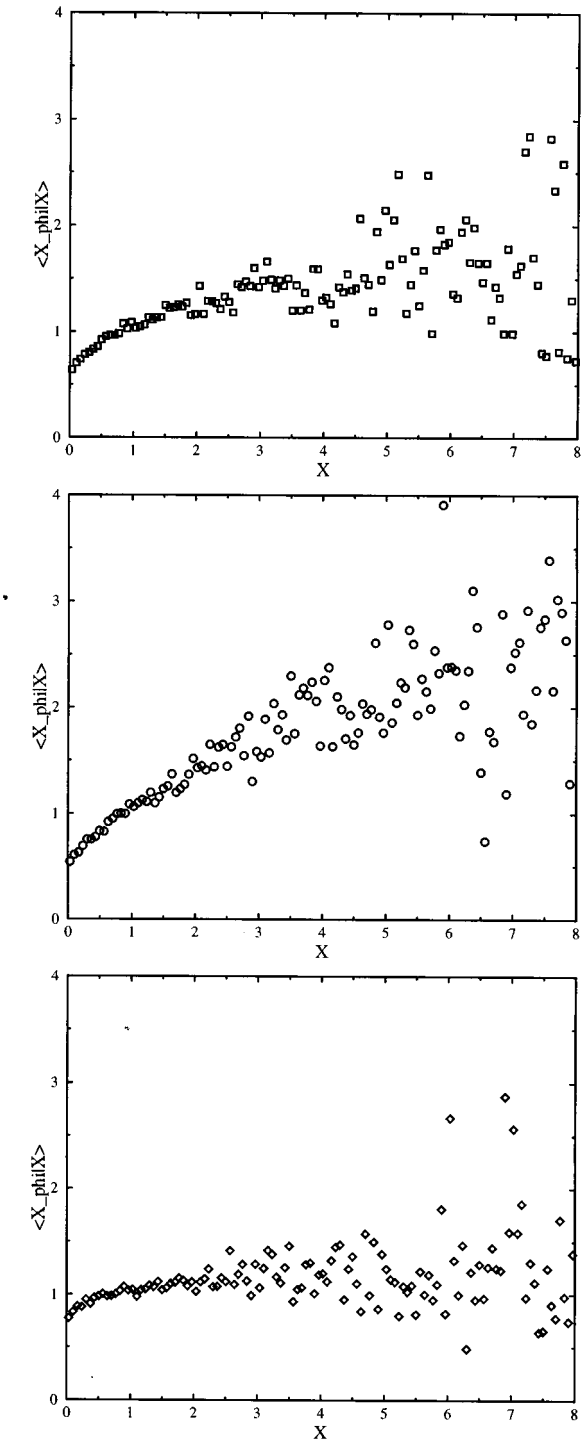

FIG. 13. Effect of the auto-correlation time of the turbulent frequency on the stationary conditional expectation of the scalar dissipation (X_ϕ) given the turbulent frequency (X) found with $R_\lambda=84$, $Sc=1$, and $N_z=1$. All other parameters are the same as in Fig. 1. □: $C_\chi=1/Re_1$; ○: $C_\chi=1$; ◇: $C_\chi=10$.

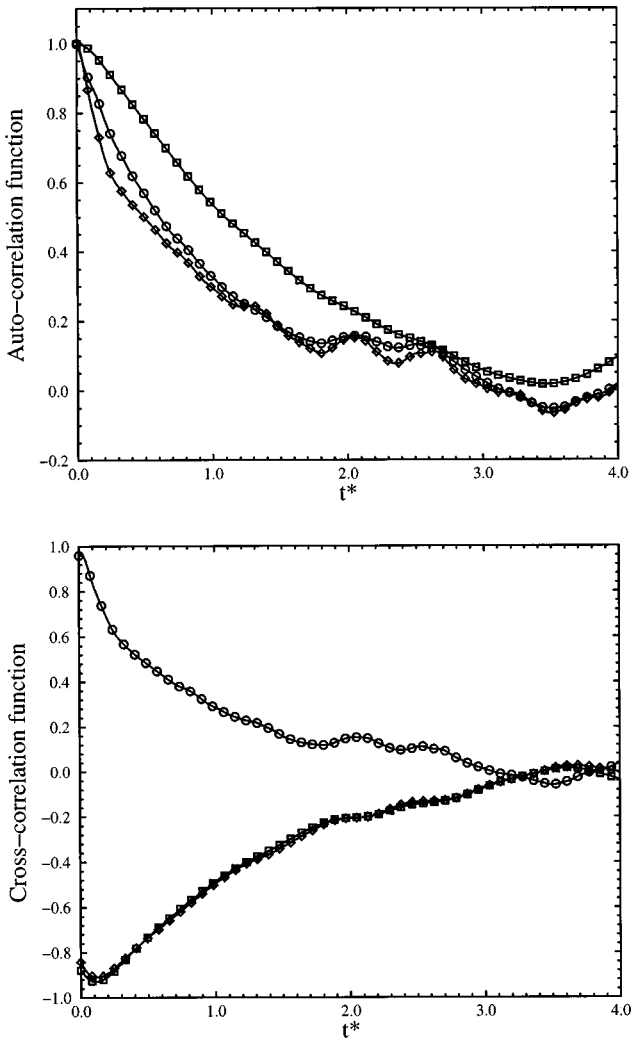

FIG. 14. Lagrangian auto- and cross-correlation functions with $C_\chi = 1/Re_1$ and all other parameters are as in Fig. 12. (Note the change in the time scale.) Top—○: ω^*; ◇: $\omega_\phi^\dagger$; □: Φ. Bottom—○: ω^* and $\omega_\phi^\dagger$; ◇: $\omega_\phi^\dagger$ and Φ; □: ω^* and Φ.

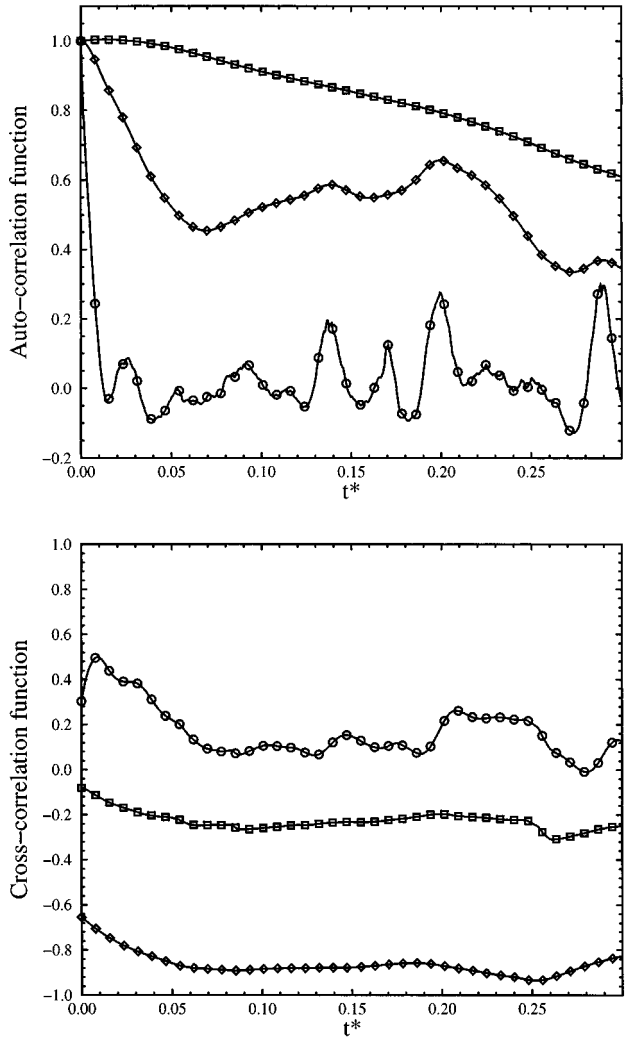

FIG. 15. Lagrangian auto- and cross-correlation functions with $C_\chi = 10$ and all other parameters are as in Fig. 12. Top—○: ω^*; ◇: $\omega_\phi^\dagger$; □: Φ. Bottom—○: ω^* and $\omega_\phi^\dagger$; ◇: $\omega_\phi^\dagger$ and Φ; □: ω^* and Φ.

become uncorrelated from ω^*, and the latter behaves more and more like a delta-correlated random process (i.e., the ''white-noise'' limit employed in earlier studies[47,48]). For good agreement with the DNS data, it is thus important that the auto-correlation time of ω^* be larger than the characteristic scalar-dissipation diffusion time $[1/(C_d\langle r\rangle_o^\dagger) \propto 1/Re_1]$ in the LSR model (compare this conclusion with those concerning the white-noise limit in Holzer and Sigga[60]). The auto- and cross-correlation functions presented in Figs. 14 and 15 confirm these observations. Additionally, as can be seen from Fig. 14, when $C_\chi \sim 1/Re_1$ the cross-correlation between $\omega(t^*)$ and $\omega_\phi^\dagger(t^*)$ is positive and nearly unity, implying that $\omega_\phi^\dagger$ is nearly a deterministic increasing function of ω^*. The DNS results[21] (with a uniform mean scalar gradient) for $\langle X_\phi | X = x\rangle$ at $R_\lambda = 84$ display a limiting value for large x of approximately 2.4 which agrees well with limiting expression given above with $\langle 1/\omega_\phi^\dagger\rangle \approx 1.4$. The latter is slightly larger than the LSR model prediction of $\langle 1/\omega_\phi^\dagger\rangle = 1.13$ with $C_\chi = 1/Re_1$, suggesting that the appropriate value of C_χ lies near the left-hand side of the interval $(1/Re_1, 1)$.

From the above results, we can conclude that for stationary isotropic turbulence (i) the scalar and scalar dissipation statistics predicted by the LSR model are in satisfactory agreement with available DNS data; (ii) the role of ''small-scale intermittency'' of the scalar dissipation (viz., turbulent frequency) in the generation of non-Gaussian scalar statistics is consistent with other studies;[50,60] (iii) the model predictions are fairly insensitive to the auto-correlation time, provided $C_\chi \leqslant 1$; (iv) the scalar dissipation moments found with $C_\chi \approx 1$ agree best with DNS, but agreement is adequate when $C_\chi \sim 1/Re_1$; (v) the conditional scalar dissipation found with $C_\chi = 1/Re_1$ agrees most closely with DNS; (vi) DNS results for the conditional scalar dissipation with $S_{\phi^2} = 0$ would be useful for determining if $C_\chi \sim 1/Re_1$ in the turbulent frequency model; (vii) experimental measurements of Lagrangian conditional scalar statistics in high-Sc flows may be useful for validating the statistics of Φ and the diffusive-mixing model; and (viii) detailed Lagrangian DNS statistics for the scalar quantities are needed to further validate the temporal statistics predicted by the LSR model.

B. Transient scalar statistics in stationary, isotropic turbulence

The second case, unlike the first which dealt with small-scale (presumably universal) phenomena, is strongly dependent upon the initial conditions of the large scales and, hence, will be highly flow dependent. Due to this dependence on large scales, experimental[62] and DNS[22] results for transient statistics for such flows are often plagued by the effects of an inadequate sample size (i.e., over a sufficient number of integral length scales), leading to large statistical fluctuations.[59] This fact makes detailed quantitative comparisons with experimental/DNS data difficult. Nevertheless, a qualitative comparison with the LSR model is possible, and will suffice to illustrate the model's ability to capture non-Gaussian scalar behavior due to large-scale inhomogeneities.

1. Model problem

In the model problem to be considered, we will again assume the turbulence to be fully developed, isotropic, and stationary. The scalar spectrum, on the other hand, will be assumed to be initially out of equilibrium so that transient scalar statistics result as it relaxes to a fully developed form. In the LSR model, this implies that the dynamic variables (e.g., $\langle \varsigma_{i,j} \rangle^\dagger$) must be initialized to represent the desired initial scalar spectrum. In the DNS[22] study that will be used for a qualitative model comparison, the most significant non-Gaussian behavior is found when the initial scalar spectrum is bimodal with one strong peak at small wavenumbers ($0 < \kappa \ll \kappa_0$) and a second at relatively high wavenumbers ($\kappa_0 \ll \kappa < \kappa_U$). In the LSR model, this would correspond to initializing all spectral fractions, except $\langle \varsigma_1 \rangle^\dagger$ and $\langle \varsigma_{2,n_2} \rangle^\dagger$, to zero. [Note that $\omega_\phi^\dagger$ must also be initialized and, theoretically, is quite arbitrary since an infinitesimal amount of scalar energy placed at a very large wavenumber could result in $\langle \varsigma_D \rangle^\dagger \approx 0$, but $\omega_\phi^\dagger \sim 1$. Its initialization, however, is of little consequence since it rapidly ($t^* \sim 1/Re_1$) relaxes to a quasi-SS value determined, primarily, by the scalar flux from large scales.] Nevertheless, since in the LSR model all large scales are ''lumped'' into stage 1 and treated as a simple source of scalar energy, care must be taken when applying the model to flows dominated by large scales. In practice, at least three possibilities present themselves for handling such flows.

(1) As noted in Sec. II, the large scales can be simulated separately (e.g., LES) up to a cut-off wavenumber, κ_c, located somewhere in the inertial subrange (stage 2). The LSR model could then be applied as a subgrid model with the scalar flux at κ_c provided as model input.

(2) The large scales can be treated using classical ''turbulent diffusivity'' (or scalar flux) models (e.g., standard Lagrangian pdf methods) on a computational grid of size $L \approx 2\pi/\kappa_0$. Large-scale scalar structures would then fall across one or more grid cells (hereinafter called region 1) and all notional particles within this region would be initialized with $\langle \varsigma_1 \rangle^\dagger = 1$. Likewise, a region of small-scale structures (region 2) could coexist between the large-scale structures, and within this region $\langle \varsigma_{2,n_2} \rangle^\dagger = 1$ (or whatever initialization that is appropriate for a given initial scalar spectrum). Notional particles with different initializations would then be advected between the grid cells, and the inertial- and diffusive-mixing terms (e.g., $\mathscr{T}_\phi$ and $\mathscr{D}_\phi$, respectively) in the LSR model would serve to ''homogenize'' the scalar field at all scales.

(3) Since the DNS simulations are homogeneous on large scales ($L \ll l$), the spatial mixing by ''turbulent diffusion'' can be approximated by splitting the notional particles into two sets (i.e., regions 1 and 2), and, for the n_i particles in set i, by replacing the unconditional means in the LSR model by weighted means, e.g.,

$$\langle \varsigma_1 \rangle^i = w_{i,1}(t^*)\langle \varsigma_1 \rangle_1 + w_{i,2}(t^*)\langle \varsigma_1 \rangle_2,$$

where $\langle \cdot \rangle_i$ is the (conditional) expected value computed using only those particles in set i. Then, taking the characteristic large-scale mixing time to be $1/\langle \omega \rangle$, the weights become

$$w_{1,1}(t^*) = \frac{1}{n_1 + n_2}(n_1 + n_2 e^{-t^*}),$$

$$w_{2,2}(t^*) = \frac{1}{n_1 + n_2}(n_2 + n_1 e^{-t^*}),$$

and $w_{i,2} = 1 - w_{i,1}$. This is the method that we shall employ in the sequel with $n_1 = n_2$ (regions of equal volume), and the initial conditions given in Table X. [The ''global average'' in Table X is defined by $\langle \cdot \rangle = (n_1\langle \cdot \rangle_1 + n_2\langle \cdot \rangle_2)/(n_1 + n_2)$.]

In the simulations, two sets of initial conditions will be considered (Table X). The first, denoted by IC1, corresponds to an initial scalar spectrum with one-half of the energy at large scales, and the other half at small scales (the total initial scalar energy is arbitrarily set to unity). IC1 thus models the double-hat DNS initial conditions of Jaberi *et al.*[22] The second set, denoted by IC2, employs the same spectral fractions, but assumes that region 1 (large scales) has a much smaller

TABLE IX. Stationary moments of the pdf of the scalar dissipation (X_ϕ) and selected statistics found with $R_\lambda = 84$, $Sc = 1$, $N_z = 1$, and $S_{\phi^2} = 1$ for selected values of the auto-correlation time of the turbulent frequency [C_χ in Eq. (58)]. Simulations run with 10^5 notional particles.

C_χ	$1/Re_1$	1	$10Re_1$	DNS
Variance	2.18	2.70	1.94	5.68 ± 2.17
Skewness	3.26	4.70	3.20	6.89 ± 0.61
Kurtosis	20.6	48.2	20.6	84.2 ± 16.8
Superskewness	1750	14400	1830	28600 ± 12200
$\langle r \rangle$	1.82	1.95	1.89	2.22
$\rho(\epsilon, \epsilon_\phi)$	0.130	0.217	0.055	0.165
σ_Φ	0.179	0.120	0.042	⋯

TABLE X. Non-equilibrium spectral initial conditions for IC1 and IC2 with $R_\lambda = 84$ and $Sc = 1$. All other parameters are as in Tables I and III. Initial conditions for remaining model variables: $\Phi = 1$, $\langle \varsigma_{2,1} \rangle^\dagger = \langle \varsigma_{2,2} \rangle^\dagger = 0$.

	IC1 $\langle \phi'^2 \rangle^i$	IC2 $\langle \phi'^2 \rangle^i$	$\langle \varsigma_1 \rangle^\dagger$	$\langle \varsigma_{2,3} \rangle^\dagger$	$\omega_\phi^\dagger$
Region 1	1.0	0.04	1.0	0.0	0.0
Region 2	1.0	1.96	0.0	1.0	6.0
Global average	1.0	1.0	0.5	0.5	3.0

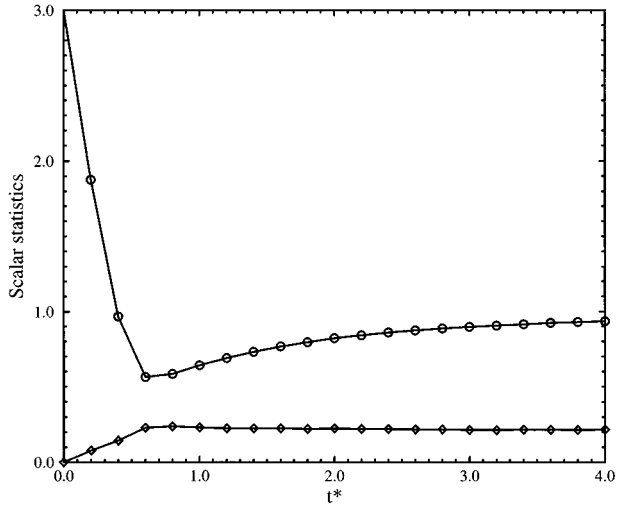

FIG. 16. Evolution of the scalar dissipation rate and the scalar-mechanical dissipation correlation coefficient with non-equilibrium spectral initial conditions, $R_\lambda = 84$, $Sc = 1$, and $N_z = 1$. ○: $\langle r_\phi \rangle$; ◇: $\rho(\epsilon, \epsilon_\phi)$. One Kolmogorov time for this flow corresponds to $t^* = 0.031$.

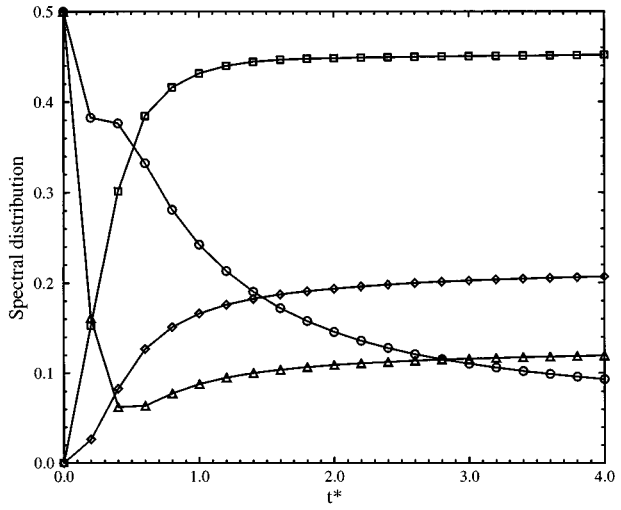

FIG. 17. Evolution of the spectral distribution with non-equilibrium spectral initial conditions. ○: $\langle s_1 \rangle$; □: $\langle s_{2,1} \rangle$; ◇: $\langle s_{2,2} \rangle$; △: $\langle s_{2,3} \rangle$. All parameters are the same as in Fig. 16.

spectral energy than region 2. In physical space, IC2 would correspond to large areas with nearly zero scalar fluctuations (region 1), separated by areas with high scalar fluctuations over short length scales (region 2). This type of scalar field has been observed in earlier numerical studies of scalar mixing,[50,60] and is seen experimentally in grid turbulence where scalar fluctuations are generated by line (grid) sources separated by approximately one integral scale.[62] For both sets of initial conditions, we will again assume that the scalar and scalar gradient fields are initially Gaussian (with a possibility different variance for each region), and that all notional particles have initially $\Phi = 1$. In addition, the effect of including a mean scalar gradient on the non-Gaussian behavior will be considered.

2. Evolution of the scalar spectrum

Figures 16 and 17 have been included to illustrate the LSR model's prediction of transient scalar spectrum. Since the results are qualitatively similar for both IC1 and IC2, only one set of curves has been included in the figures. In Fig. 16, the evolution of $\langle r_\phi \rangle$ and $\rho(\epsilon, \epsilon_\phi)$ is presented and can be divided into two distinct time periods. The first period ($t^* < 0.5$) is dominated by the fast relaxation of the small scales and, during this period, most of the spectral energy at small scales (i.e., in region 2) dissipates. The second period ($0.5 < t^*$) is dominated by the slow relaxation of large scales, the homogenization of the scalar field by ''turbulent diffusion,'' and the gradual approach to spectral equilibrium. Note that the dimensionless Kolmogorov time scale for this flow is $t_K = 0.031$ and, hence, the first period is relatively long. (Nevertheless, its length is proportional to the characteristic time scale of the small scales: $t_{2,3} = 0.125/\langle \omega \rangle$.) The spectral fractions, appearing in Fig. 17, display a similar behavior and are consistent with the DNS results (compare with Fig. 11 in Jaberi *et al.*[22]). Finally, note that scalar dissipation statistics [viz., $\rho(\epsilon, \epsilon_\phi)$] reach their final values relatively quickly due to the fact that the characteristic time scale of scalar dissipation is proportional to $1/Re_1$ in the LSR model ($C_\chi = 1$).

3. Evolution of the scalar pdf

The evolution of the superskewness of the scalar pdf is shown in Fig. 18. From these curves it can be seen that the transient scalar pdf is highly non-Gaussian, especially in the absence of a mean scalar gradient, relaxing to a self-similar form only after $t^* \approx 3$. By construction, the scalar pdf for IC1 is initially Gaussian; however, since the large and small scales have the same fraction of the total spectral energy, it rapidly becomes non-Gaussian due to the loss of spectral energy in the small scales (i.e., the scalar variance in region 2 decreases much faster than that in region 1). The scalar pdf

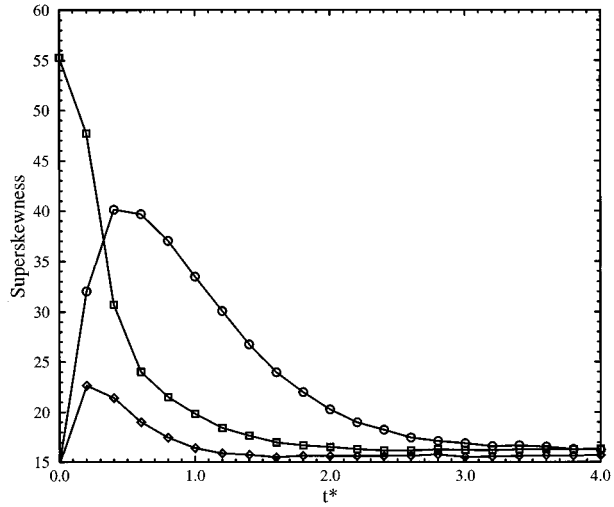

FIG. 18. Evolution of the scalar superskewness with non-equilibrium spectral initial conditions. ○: IC1 with $S_{\phi^2} = 0$; ◇: IC1 with $S_{\phi^2} = 1$; □: IC2 with $S_{\phi^2} = 0$; Gaussian value: 15.

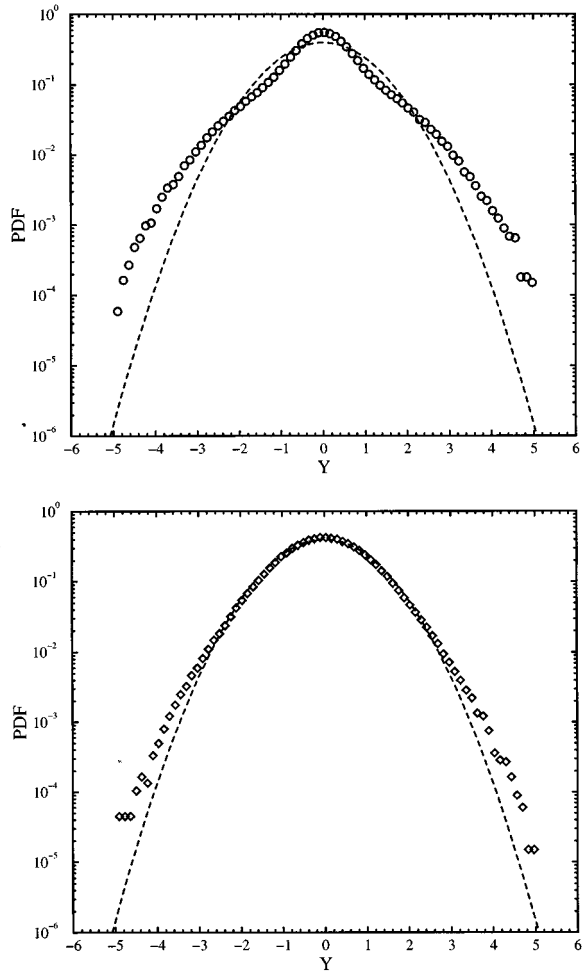

FIG. 19. Scalar pdf at $t^*=0.4$ for IC1. ○: $S_{\phi^2}=0$; ◇: $S_{\phi^2}=1$. Dashed curves: Gaussian pdf.

for IC2, on the other hand, is initially highly non-Gaussian, but evolves towards a Gaussian form by the same mechanism. The large effect of the presence of a mean scalar gradient is also evident in the figure where it can be seen that the maximum deviation from Gaussian behavior is over three times larger when $S_{\phi^2}=0$ than when $S_{\phi^2}=1$. Scalar pdf at $t^*=0.4$, presented in Fig. 19, further illustrate the strong ''smoothing'' effect of a mean scalar gradient. Nearly identical behavior is seen from DNS.[22] The essential difference between zero- and uniform mean scalar gradient results is the fact the latter has a Gaussian scalar variance source term [Eq. (92)] that is uniform in both regions. Thus, as the initial scalar energy dissipates away, it is quickly (and uniformly) replenished until both regions are statistically identical at all scales. Note that, in addition, if the source term produced regions where the scalar variance and spectral distribution were *correlated* (e.g., the ''ramp-and-cliff'' structures seen in uniform mean gradient studies[50,60,63]), then the scalar pdf would be further modified from the Gaussian form. In principle, the LSR model is applicable to such flows; however, the conditional scalar variance source model [Eq. (92)] would need to be modified to account for the correlations.

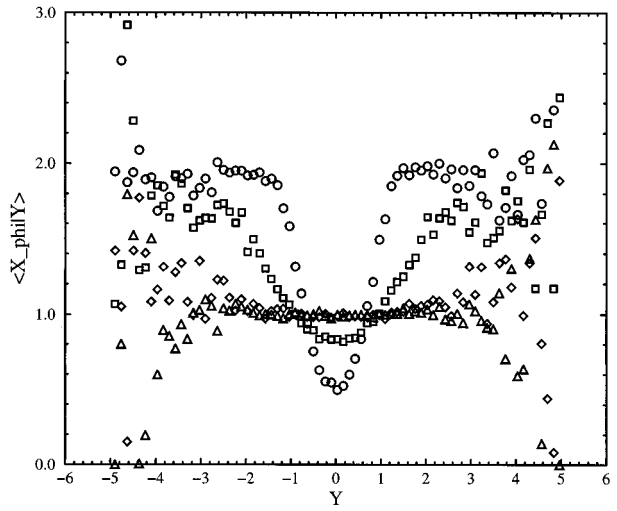

FIG. 20. Conditional expectation of the scalar dissipation (X_ϕ) given the scalar (Y) for IC2 with $S_{\phi^2}=0$. ○: $t^*=0.2$; □: 0.4; ◇: 0.8; △: 1.6.

4. Evolution of conditional scalar statistics

The role of the various unclosed terms in the Lagrangian scalar pdf equation [Eq. (83)] in the production of transient non-Gaussian scalar pdf can be highlighted by computing the conditional scalar dissipation $\langle X_\phi | Y=x\rangle$, the conditional scalar Laplacian $\langle D|Y=x\rangle$, and the conditional scalar flux,

$$\langle A|Y=x\rangle=\left\langle \frac{\mathbf{u}\cdot\nabla\phi'}{\langle\omega\rangle\sigma_\phi}\middle|\frac{\phi'^*}{\sigma_\phi}=x\right\rangle.$$

As noted earlier, if all three functions are linear in x, then the scalar pdf will be Gaussian. These quantities, computed from the LSR model at four different times for IC2 with $S_{\phi^2}=0$, appear in Figs. 20–22, respectively. Looking first at the conditional scalar dissipation, note that it displays the parabolic form found in grid turbulence[62] and is often taken as a telltale sign of non-Gaussian behavior.[50,60] (It is, however, not a

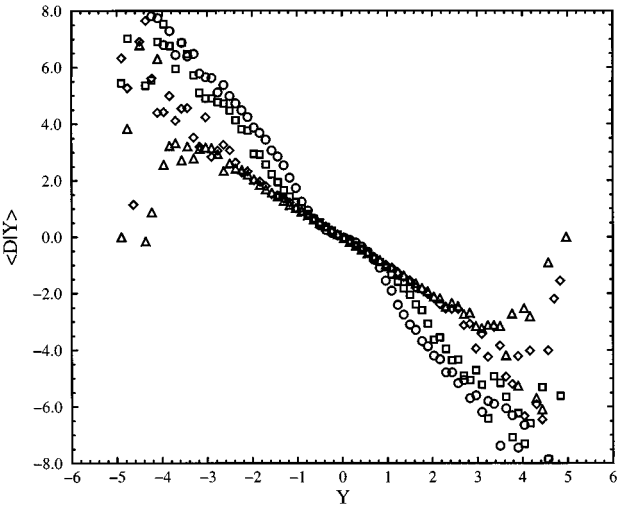

FIG. 21. Conditional expectation of the scalar Laplacian $[D=(\Gamma\nabla^2\phi')/(\langle r_\phi\rangle\sigma_\phi)]$ given the scalar (Y) for IC2 with $S_{\phi^2}=0$. ○: $t^*=0.2$; □: 0.4; ◇: 0.8; △: 1.6.

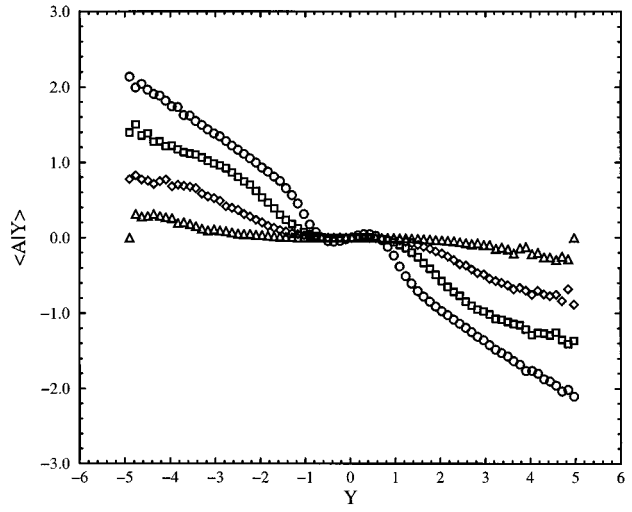

FIG. 22. Conditional expectation of scalar flux $[A=(\mathbf{u}\cdot\nabla\phi')/(\langle\omega\rangle\sigma_\phi)]$ given the scalar (Y) for IC2 with $S_{\phi^2}=0$. ○: $t^*=0.2$; □: 0.4; ◇: 0.8; △: 1.6.

necessary condition since the transient conditional dissipation for IC1 has an *inverted*-parabolic form!) The appearance of a parabolic form for IC2 is easily understood from the initial conditions: large scalar fluctuations are initially correlated with large scalar dissipation. The conditional scalar Laplacian (Fig. 21) and the conditional scalar flux [Eq. (22)] also display strongly non-linear forms, and also behave differently for different initial conditions. (The former is often modeled as a linear function, even in cases where the scalar pdf is highly non-Gaussian.[19]) Neither of these quantities are available from the DNS study[22] for comparison with the model, but both would be particularly useful for model validation and improvement. It would be important, however, to measure them all for exactly the same flow at the same time instant since their forms are highly dependent on the initial conditions.

From the above results, we can conclude that large-scale inhomogeneities in the initial scalar spectral distribution have a strong and sustained effect on the evolution of the scalar field statistics, and that these effects are successfully captured by the LSR model. Future DNS/experimental studies of such flows are urged to report conditional scalar statistics, in particular, $\langle A|Y=x\rangle$, in order to allow for a more complete validation of the inertial-range mixing term in the LSR model.

V. CONCLUSIONS

A Lagrangian pdf version of the spectral relaxation model for the scalar dissipation rate in homogeneous turbulent flows has been derived and verified against DNS data. The Lagrangian spectral relaxation model differs from single time-scale models by the inclusion of multiple turbulence time scales through a simple description of the cascade of scalar energy from large to small scales, and by the appearance on the instantaneous turbulent frequency to describe the vortex-stretching history of the fluid particle. Based on the comparisons with DNS, it is clear that the model for the turbulent frequency plays an important role in the overall satisfactory agreement of the scalar field statistics. In particular, it was shown that a stretched-exponential form for the scalar dissipation pdf results only in the case where the turbulent frequency pdf is also stretched exponential, that the auto-correlation time of the turbulent frequency strongly influences the joint statistics, and that the mean turbulent frequency has a significant effect on the equilibrium mean scalar dissipation rate. Further improvement in scalar-dissipation models in general will thus depend directly on improvements in the turbulent frequency model (e.g., in the description of non-equilibrium effects and of large scales).

The field of application of the Lagrangian spectral relaxation model can be extended in various ways beyond the simple homogeneous flows considered in the present work. In its current form, the model is directly applicable to the study of differential diffusion of passive scalars in homogeneous turbulence.[30] With minor modifications, it should also be possible to apply the model to the study of the important areas of homogeneous non-premixed turbulent reacting flows near extinction, inhomogeneous scalar mixing problems, and premixed turbulent combustion.[64] Furthermore, application of the model to the description of small-scale mixing (micromixing) in the chemical process industry[11] should be particularly fruitful due to the relative abundance of flows far from scalar-spectral equilibrium (e.g., reacting point source in a fully developed turbulent jet[65,66] or in a fully developed turbulent pipe flow[24]).

Note added in proof. The most recent version of the model employs the following definitions of the molecular dissipation rate: $\langle r_\phi\rangle_0=\langle\epsilon_\phi\rangle/\langle\phi_D'^2\rangle$ and $\langle r_\phi\rangle^+=\langle\epsilon_\phi\rangle^*/\langle\phi_D'^2\rangle^*$.

ACKNOWLEDGMENTS

This work was supported by the National Science Foundation under Grant No. CTS-9158124 (PYI Award) and The Dow Chemical Company. The author would also like to acknowledge the Center National de la Recherche Scientifique (CNRS) and the Université de Rouen, France for sabbatical-leave support during the final phase of the project.

[1] S. Corrsin, ''The isotropic turbulent mixer: Part II. Arbitrary Schmidt number,'' AIChE J. **10**, 870 (1964).
[2] G. R. Newman, B. E. Launder, and J. L. Lumley, ''Modelling the behaviour of homogeneous scalar turbulence,'' J. Fluid Mech. **111**, 217 (1981).
[3] S. B. Pope, ''Pdf methods for turbulent reactive flows,'' Prog. Energy Combust. Sci. **11**, 119 (1985).
[4] R. O. Fox, ''The spectral relaxation model of the scalar dissipation rate in homogeneous turbulence,'' Phys. Fluids **7**, 1082 (1995).
[5] K. Tsai and R. O. Fox, ''Modeling the scalar dissipation rate for a series-parallel reaction,'' Chem. Eng. Sci. **50**, 1929 (1996).
[6] R. W. Bilger, ''Turbulent diffusion flames,'' Annu. Rev. Fluid Mech. **21**, 101 (1989).
[7] Z. Warhaft and J. L. Lumley, ''An experimental study of the decay of temperature fluctuations in grid-generated turbulence,'' J. Fluid Mech. **88**, 659 (1978).
[8] A. Sirivat and Z. Warhaft, ''The effect of a passive cross-stream temperature gradient on the evolution of temperature variance and heat flux in grid turbulence,'' J. Fluid Mech. **128**, 323 (1983).
[9] R. J. Brown and R. W. Bilger, ''An experimental study of a reactive plume in grid turbulence,'' J. Fluid Mech. **312**, 373 (1996).
[10] V. Eswaran and S. B. Pope, ''Direct numerical simulations of the turbulent mixing of a passive scalar,'' Phys. Fluids **31**, 506 (1988).

[11]R. O. Fox, ''Computational methods for turbulent reacting flows in the chemical process industry,'' Rev. Inst. Français Pétrole **51**, 215 (1996).
[12]S. B. Pope, ''Lagrangian pdf methods for turbulent flows,'' Annu. Rev. Fluid Mech. **26**, 23 (1993).
[13]A. R. Masri, R. W. Dibble, and R. S. Barlow, ''Chemical kinetic effects in nonpremixed flames of H_2/CO_2 fuel,'' Combust. Flame **91**, 285 (1992).
[14]J.-Y. Chen and W. Kollman, ''Pdf modeling of chemical nonequilibrium effects in turbulent nonpremixed hydrocarbon flames,'' *22nd Symposium (International) on Combustion* (The Combustion Institute, Pittsburgh, 1988), pp. 645–653.
[15]S. Taing, A. R. Masri, and S. B. Pope, ''Pdf calculations of turbulent nonpremixed flames of H_2/CO_2 using reduced chemical mechanisms,'' Combust. Flame **95**, 133 (1993).
[16]A. T. Norris and S. B. Pope, ''Modeling of extinction in turbulent diffusion flames by the velocity-dissipation-composition pdf method,'' Combust. Flame **100**, 211 (1995).
[17]Y. Y. Lee and S. B. Pope, ''Nonpremixed turbulent reacting flow near extinction,'' Combust. Flame **101**, 501 (1995).
[18]S. Mahalingam, J. H. Chen, and L. Vervisch, ''Finite-rate chemistry and transient effects in direct numerical simulations of turbulent nonpremixed flames,'' Combust. Flame **102**, 285 (1995).
[19]R. O. Fox, ''The Fokker–Planck closure for turbulent molecular mixing: Passive scalars,'' Phys. Fluids A **4**, 1230 (1992).
[20]R. O. Fox, ''Improved Fokker–Planck model for the joint scalar, scalar gradient pdf,'' Phys. Fluids **6**, 334 (1994).
[21]M. R. Overholt and S. B. Pope, ''DNS of a passive scalar with imposed mean gradient in isotropic turbulence,'' Phys. Fluids **8**, 3128 (1996).
[22]F. A. Jaberi, R. S. Miller, C. K. Madnia, and P. Givi, ''Non-Gaussian scalar statistics in homogeneous turbulence,'' J. Fluid Mech. **313**, 241 (1996).
[23]K. Tsai and R. O. Fox, ''Pdf simulation of a turbulent series-parallel reaction in an axisymmetric reactor,'' Chem. Eng. Sci. **49**, 5141 (1994).
[24]K. Tsai and R. O. Fox, ''Pdf modeling of turbulent-mixing effects on initiator efficiency in a tubular LDPE reactor,'' AIChE J. **42**, 2926 (1996).
[25]M. Pipino and R. O. Fox, ''Reactive mixing in a tubular jet reactor. A comparison of pdf simulations with experimental data,'' Chem. Eng. Sci. **49**, 5229 (1994).
[26]G. K. Batchelor, ''The effect of homogeneous turbulence on material lines and surfaces,'' Proc. R. Soc. London, Ser. A **213**, 349 (1952).
[27]G. K. Batchelor, ''Small-scale variation of convected quantities like temperature in turbulent fluid. Part 1. General discussion and the case of small conductivity,'' J. Fluid Mech. **5**, 113 (1959).
[28]R. O. Fox, J. C. Hill, F. Gao, R. D. Moser, and M. M. Rogers, ''Stochastic modeling of turbulent reacting flows'' in *Proceedings of the 1992 Summer Program* (Center for Turbulence Research, Stanford, 1992).
[29]P. K. Yeung, ''Spectral transport of self-similar passive scalar fields in isotropic turbulence,'' Phys. Fluids **6**, 2245 (1994).
[30]P. K. Yeung, ''Multi-scalar triadic interactions in differential diffusion with and without mean scalar gradients,'' J. Fluid Mech. **321**, 235 (1996).
[31]A. N. Kolmogorov, ''The local structure of turbulence in incompressible viscous fluid for very large Reynolds numbers,'' Dokl. Akad. Nauk SSR **30**, 301 (1941).
[32]A. M. Obukhov, ''Structure of the temperature field in turbulent flows,'' Izv. Akad. Nauk SSSR, Ser. Geogr. Geofiz. **13**, 58 (1949).
[33]S. Corrsin, ''On the spectrum of isotropic temperature fluctuations in isotropic turbulence,'' J. Appl. Phys. **22**, 469 (1951).
[34]S. B. Pope, *Turbulent Flows* (Cambridge University Press, Cambridge, in press).
[35]C. E. Leith, ''Diffusion approximation to inertial energy transfer in isotropic turbulence,'' Phys. Fluids **10**, 1409 (1967).
[36]D. C. Besnard, F. H. Harlow, R. M. Rauenzahn, and C. Zemach, ''Spectral transport model for turbulence,'' Report No. LA-UR92-1666, Los Alamos National Laboratory, 1992.
[37]T. T. Clark and C. Zemach, ''A spectral model applied to homogeneous turbulence,'' Phys. Fluids **7**, 1674 (1995).
[38]C. Meneveau and T. S. Lund, ''On the Lagrangian nature of the turbulence energy cascade,'' Phys. Fluids **6**, 2820 (1994).
[39]C. Meneveau, T. S. Lund, and W. H. Cabot, ''A Lagrangian dynamic subgrid-scale model of turbulence,'' J. Fluid Mech. **319**, 353 (1996).
[40]M. S. Borgas and B. L. Sawford, ''Stochastic equations with multifractal random increments for modeling turbulence dispersion,'' Phys. Fluids **6**, 618 (1994).
[41]S. B. Pope and Y. L . Chen, ''The velocity-dissipation probability density function model for turbulent flows,'' Phys. Fluids A **2**, 1437 (1990).
[42]S. B. Pope, ''Application of the velocity-dissipation probability density function model to inhomogeneous turbulent flows,'' Phys. Fluids A **3**, 1947 (1991).
[43]W. Feller, *An Introduction to Probability Theory and Its Applications*, 2nd ed. (Wiley, New York, 1971).
[44]R. O. Fox, ''On velocity-conditioned scalar mixing in homogeneous turbulence,'' Phys. Fluids **8**, 2678 (1996).
[45]S. B. Pope, ''On the relationship between stochastic Lagrangian models of turbulence and second-moment closures,'' Phys. Fluids **6**, 973 (1993).
[46]E. Gledzer, E. Villermaux, H. Kahalerras, and Y. Gagne, ''On the log-Poisson statistics of the energy dissipation field and related problems of developed turbulence,'' Phys. Fluids **8**, 3367 (1996).
[47]R. E. Meyers and E. E. O'Brien, ''The joint pdf of a scalar and its gradient at a point in a turbulent flow,'' Combust. Sci. Technol. **26**, 123 (1981).
[48]L. Valiño and C. Dopazo, ''Joint statistics of scalars and their gradients in nearly homogeneous turbulence,'' in *Advances in Turbulence 3*, edited by A. V. Johansson and P. H. Alfredsson (Springer, Berlin, 1991), p. 312.
[49]W. T. Ashurst, A. R. Kerstein, R. M. Kerr, and C. H. Gibson, ''Alignment of vorticity and scalar gradient in simulated Navier–Stokes turbulence,'' Phys. Fluids **30**, 2343 (1987).
[50]A. Pumir, ''A numerical study of the mixing of a passive scalar in three dimensions in the presence of a mean gradient,'' Phys. Fluids **6**, 2118 (1994).
[51]K. A. Buch and W. J. A. Dahm, ''Experimental study of the fine-scale structure of conserved scalar mixing in turbulent shear flows,'' J. Fluid Mech. **317**, 21 (1996).
[52]L. K. Su and W. J. A. Dahm, ''Scalar imaging velocimetry measurements of the velocity gradient tensor field in turbulent flows. II. Experimental results,'' Phys. Fluids **8**, 1883 (1996).
[53]L. Valiño and C. Dopazo, ''A binomial Langevin model for turbulent mixing,'' Phys. Fluids A **3**, 3034 (1991).
[54]K. Tsai and R. O. Fox, ''Modeling multiple reactive scalar mixing with the generalized IEM model,'' Phys. Fluids **7**, 2820 (1995).
[55]K. Tsai and R. O. Fox, ''The beta mapping closure/GIEM model for non-premixed inhomogeneous turbulent reacting flows,'' submitted to Ind. Eng. Chem. Fundam.
[56]A. Juneja and S. B. Pope, ''A DNS study of turbulent mixing of two passive scalars,'' Phys. Fluids **8**, 2177 (1996).
[57]A. Sahay and E. E . O'Brien, ''Uniform mean scalar gradient in grid turbulence: Conditioned dissipation and production,'' Phys. Fluids A **5**, 1076 (1993).
[58]X. D. Cai, E. E. O'Brien, and F. Ladeinde, ''Uniform mean scalar gradient in grid turbulence: Asymptotic probability distribution of a passive scalar,'' Phys. Fluids **8**, 2555 (1996).
[59]M. R. Overholt and S. B. Pope, ''A deterministic forcing scheme for direct numerical simulations of turbulence,'' preprint (1996).
[60]M. Holzer and E. D. Siggia, ''Turbulent mixing of a passive scalar,'' Phys. Fluids **6**, 1820 (1994).
[61]P. K. Yeung and S. B. Pope, ''Lagrangian statistics from direct numerical simulations of isotropic turbulence,'' J. Fluid Mech. **207**, 531 (1989).
[62]Jayesh and Z. Warhaft, ''Probability distributions, conditional dissipation and transport of passive temperature fluctuations in grid-generated turbulence,'' Phys. Fluids A **4**, 2292 (1992).
[63]F. Anselmet, H. Djeridi, and L. Fulachier, ''Joint statistics of a passive scalar and its dissipation in turbulent flows,'' J. Fluid Mech. **280**, 173 (1994).
[64]T. Mantel and R. Borghi, ''A new model of premixed wrinkled flame propagation based on a scalar dissipation equation,'' Combust. Flame **96**, 443 (1994).
[65]J. Baldyga, J. R. Bourne, B. Dubuis, A. W. Etchells, R. V. Gholap, and B. Zimmerman, ''Jet reactor scale-up for mixing-controlled reactions,'' Trans. IChemE **73**, 497 (1995).
[66]E. Villermaux and C. Innocenti, ''Mixing times and spectral slopes,'' Récent Prog. Génie Proc. **11**, 397 (1997).